1 Theory

Most solar cells made are crystalline, meaning the structure of atoms is ordered, or periodic. Generally the crystals will contain imperfections and impurities. Some solar cell materials however, is not crystalline, but are missing periodicity. These solar cells are made from amorphous materials.

1.1 Bandgap

A free electron in vacuum is able to have any energy. An electron in a crystal is bound by an energy gap divided by energy positions the electrons can't possess. Every available energy state can only room two electrons according to the Pauli principle. For a crystal, the energy bands can be viewed as an overlap in between single electron energy states. This can be viewed as the crystals 'electron'-shell.

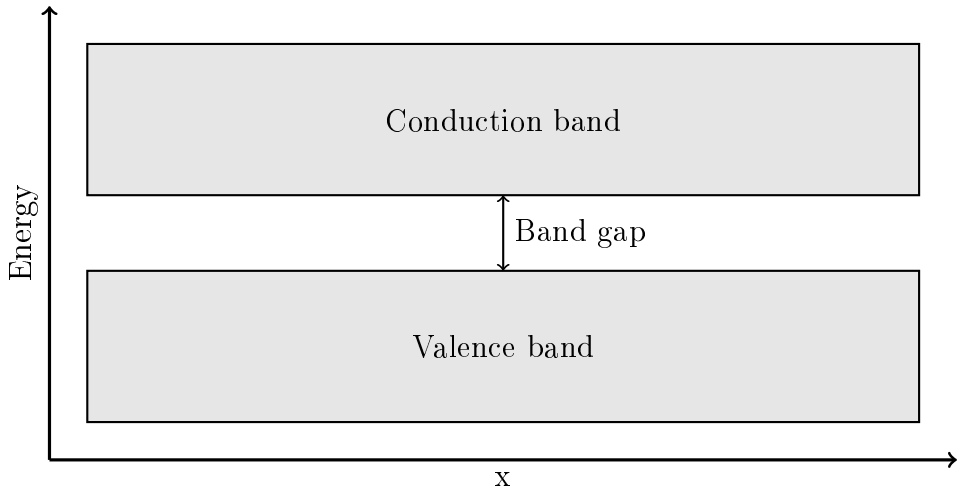

Figure 1: Energy bands

The upper band is called conduction band. The band right below it, is called the valence band. This band gap is very important in relations with solar cells, and is often given in the units of electron volts (eV).

For electrons to move out of the crystal, they have to be in the conduction band. For electrons to get to the conduction band, they need to have enough energy to move from the valence band. This can happen if the electron has enough thermal energy, or receive energy from the outside, like light. This gives the material increased conductivity. In addition to this, there will be a free state in the valence band, which results in a less probability of

collisions among the remaining electron, which lead to a higher mean kinetic energy of the electrons in the valence band. This also contribute to a better conductivity for the material.

For light to excite an electron from the valence band to the conduction band, it needs to have equal, or more energy than the band gap. Energy of light in electron volts is given by:

$$E = h\nu = \frac{hc}{\lambda} \tag{1}$$

where E is energy in electron volts, h is Planks constant, ν is frequency, and c is the speed of light.

Materials is often divided into three categories; Isolators, semiconductors, and conductors. Isolators have none, or few electrons in the conduction band, which gives them poor conductivity. Conductors often have filled conduction bands in room temperature, which provide good conductivity. Even with 0K, conductors have a partially filled conduction band. Semiconductors on the other hand, does not have any electrons in the conduction band at 0K. Semiconductors have lower conductivity than conductors, but better than isolators. The bandgap for semiconductors lay in between that of the conductors and isolators. At room temperature semiconductors have a partially filled conduction band.

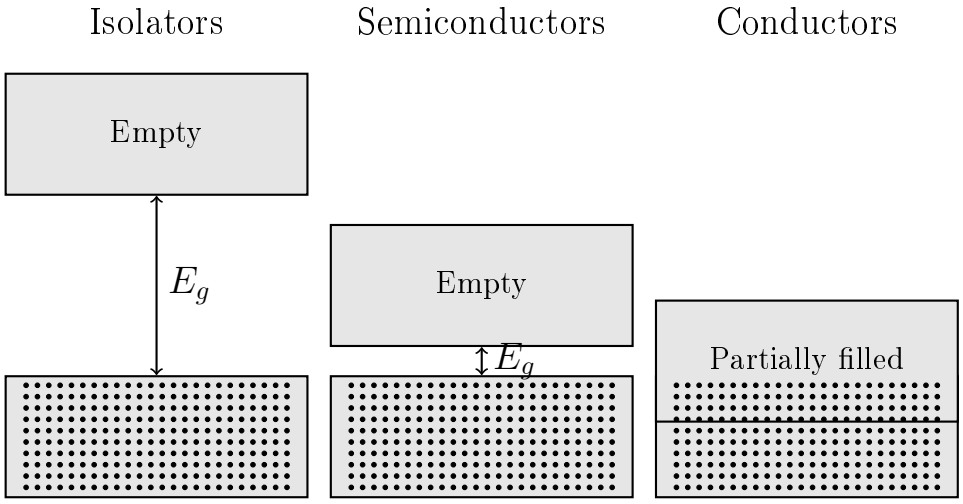

Figure 2: Typical bandgaps at 0K

Typical bandgap for semiconductor silicon is E_g=1.1 eV, compared with 5 eV for diamond, which is an isolator [1, Chapter 3].

Holes is a description of missing electrons in the valence band. A hole will appear when an electron is excited from the valence band into the conduction band. With a small bandgap, and high temperatures, there will be a considerably larger amount of electrons in the conduction band, compared to low temperatures, and a large bandgap. This is described by low of mass action

$$np = N_c N_v e^{-\frac{E_g}{kT}} \tag{2}$$

where n is number of electrons, p is number of holes, N_c and N_v is constants for a given material, E_g is the bandgap, k is Boltzmanns constant, and T is temperature in Kelvin. For an intrinsic semiconductor, meaning a semiconductor without any doping atoms, like a pure silicon crystal, the law of mass action can be written as

$$np = n_i^2 \tag{3}$$

where

$$n_i = \sqrt{N_c N_v} e^{-\frac{E_g}{2kT}} \tag{4}$$

1.2 Doping

By adding certain atoms of a different type than those constituting the semiconductor itself, it is possible in increase the concentration of electrons in the conduction band without a concomitant increase on the number of holes in the valence band. This is called donor-doping. An example of donor doping is added phosphorous into a silicon crystal. This will result in more electrons in the conduction band, due to phosphor having one more valence electron than silicon. The doping is usually so small that the band structure won't be affected. By adding phosphorous this way, one has increased electrons, n, without increasing holes, p. This is called donor doping. If you instead of phosphor, add boron, the material will be acceptor doped. This is due to boron having one less electron in the valence band than silicon, and would result in an extra hole in the valence band of the crystal. Usually the number of dopants in silicon are substantially larger than the intrinsic concentration, n_i, so that

$$n \approx N_d \tag{5}$$

for donor doping, and

$$n \approx N_a \tag{6}$$

for acceptor doping where N_d is donor concentration, and N_a is acceptor concentration.

A doped semiconductor is generally called extrinsic [1]. If a semiconductor is doped with a number of donor atoms, it is called n-doped or n-type, due to there being more electrons than holes. For acceptor doping it is called p-doped, or p-type semiconductor. The dominating charge carrier in the semiconductor are called majority carriers. The other charge carrier, i.e. holes in the n-type semiconductor are called minority carriers.

1.3 Transport and recombination processes

There are two mechanisms that contribute to transport of electrons and holes in semiconductors: drift, and diffusion. Drift is a transport of a charge carrer due to an electric field. For transport of a hole in one dimension, the current I_p is equal to the amount of holes N_p times the charge q crossing a cross-sectional area.

$$I_p = N_p q \tag{7}$$

In vacuum, an electric field would accelerate the electrons, and the velocity would increase indefinitely. In solids, however, interactions of collisions with other species in the solid leads to a resistance towards the drift of the charged particles, and after an initial acceleration the velocity becomes constant in a constant electric field. This average drive velocity, denoted v_p for holes, is related to the electric field E through the hole mobility μ_p

$$v_p = \mu_p E \tag{8}$$

If all the electrons is moving in the same direction, the current per area is given by

$$J_p = \frac{I_p}{A} = \frac{N_p q}{A} = pAv_p\frac{q}{A} = pv_p q = pq\mu_p E \tag{9}$$

combined with a similar expression for electrons

$$J = J_p + J_n = (nq\mu_n + pq\mu_p)E = \sigma E \tag{10}$$

where μ_n is the mobility for electrons,σ is the semiconductors conductivity, and J_n is the current density due to the concerted movement of electrons. It is also usual to define the resistivity of the semiconductor as the inverse of its conductivity. The current is then obtained by

$$I = JA = A\sigma E = \left(\frac{A\sigma}{L}\right) V \tag{11}$$

which is recognized as Ohm's law.

Diffusion is a transport process caused by the random motion of the diffusing particles in the medium in which they diffuse. The net transport of particles is in the opposite direction of the concentration gradient. For holes we have

$$N_p = -D_p \frac{dp}{dx} \tag{12}$$

where the proportionality constant D_p is the diffusion coefficient (m^2/s) for holes.

The movement of charged particles are frequently determined by the simultaneous presence of electric fields and concentration gradients. Both of the relevant transport parameters, mobilities and diffusion coefficients, will in general depend on temperature. The relation between diffusion coefficient and mobility is

$$\frac{D_p}{\mu_p} = \frac{kT}{q} \tag{13}$$

for holes, and a corresponding one exist for electrons.

1.4 Excitation and recombination

Electrons can move from one band to another directly, or indirectly. In indirect generation and recombination the electrons employ the so-called gap-states. Such conditions will always exist in semiconductors and are related to impurities, defects in the crystal structure, boundary surfaces (grain boundaries) and surfaces. Gap-states are in between the valence band and the conduction band, which is not allowed states in a perfect crystal.

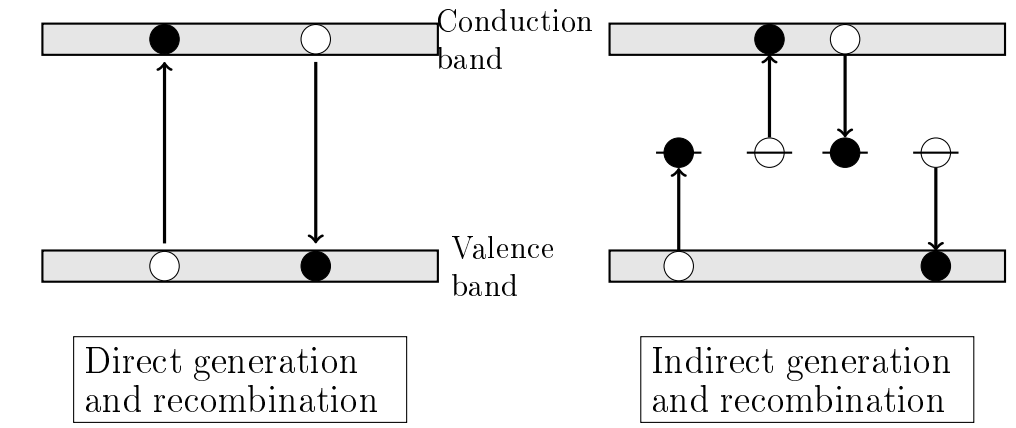

Figure 3: Generation and recombination

In semiconductors with direct bandgap, like GaAs, both processes will occur. In semiconductors with with indirect bandgap, like silicon, a direct process cannot happend without contributions from lattice vibrations (phonons), something which makes the process less probable. This is one of the reasons why impurities in silicon solar cells is an important parameter. The electron in an indirect process is moving in the form of a plane wave with propagation constant $\vec{k}$, also called wave vector.

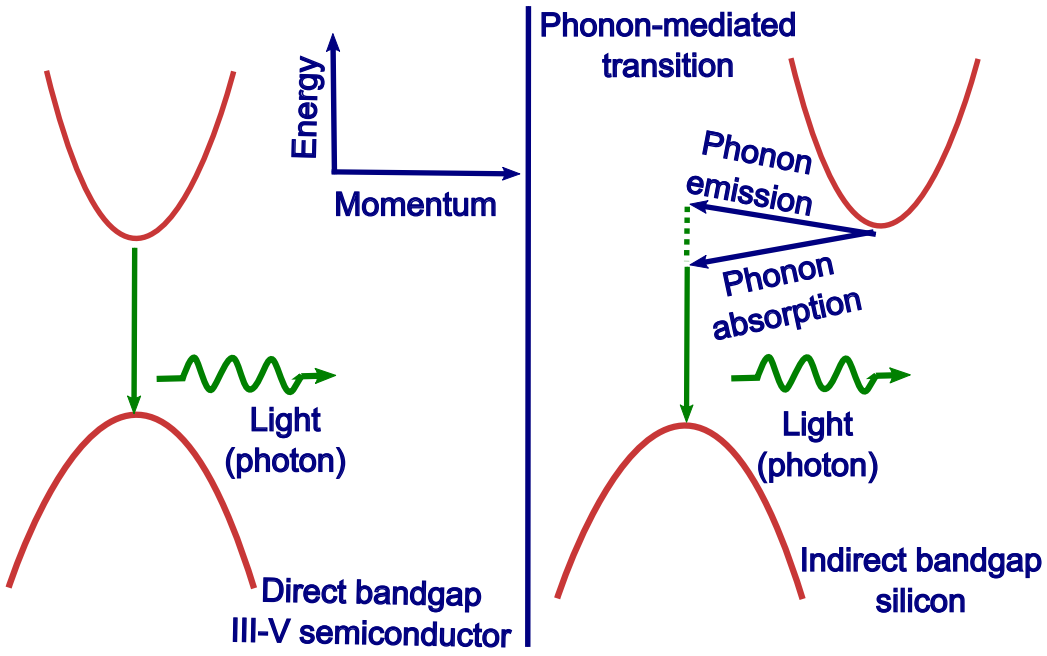

Figure 4: Direct and indirect recombination (figure from [2])

Generation and recombination processes can be described as net flow of electrons to the conduction band, U_n, proportional to the deviation from equilibrium

$$U_n = -\frac{n - n^0}{\tau_n} \tag{14}$$

where τ_n is the lifetime of electrons. n is the concentration of holes and n^0 is the equilibrium concentration of electrons, $n^0 = n_i^2$. The lifetime is the time that an electron of average speeds in the conduction band use before recombining with a hole. Similarly, the net production of holes U_p

$$U_p = -\frac{p - p^0}{\tau_p} \tag{15}$$

1.5 Solar cells

In a semiconductor with one p-doped, and one n-doped area laying next to each others is called a pn-junction. A pn-junction has rectifying properties, meaning the r electrical conductance are significantly better in one direction than the other, in contrast to a resistor for which it does not matter for the voltage drop across the resistance whether the current runs one way or another through it. This rectifying behavior defines a diode. Due to the p-side having a larger concentration of eletrons in the conduction band than the n-side, there will be a net transport of conduction band electrons from the n-side, to the p-side by diffusion. The same is also happening for holes from the p-side to the n-side. This net flow of charge is called the diffusion current. In principle, the dopants of Si, B, and P can also diffuse between the two parts of the crystal. Such a transport will only be significant at the temperature range of 800 to 900° C, and can be neglected at low temperatures like room temperature.

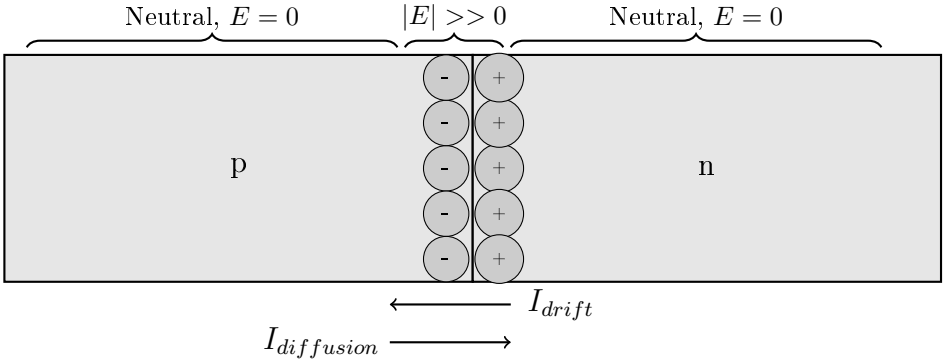

Figure 5: Depletion area

Each hole that leaves the p-side will therefor leave behind an acceptor that is no longer neutralized by a hole. Similarly, each electron in the n-side leave behind a donoor that is not neutralized by an electron. A layer near the interface between the two materials with non-neutral donors on the n-side and non-neutral acceptor in the p-side will therefor form. This layer is often called the depletion layer, since it is essentially depleted of free charge carriers. Since the n-side of the depletion layer contains non-neutral donors this side will be positively charged. The corresponding p.side will be negatively charged. These charges therefore will cause an electric field directed from n-to p-side, or a corresponding drop in electrical potential from the n-side to the p-side. This electrical potential is resulting in a drift current which is moving in the opposite direction of the diffusion current which is resulting in equilibrium, meaning zero net flow of current.

By exposing the pn-junction to light, minority carriers may be generated beyond those generated thermally. The carriers are generated by photon absorption. This generation is usually significantly greater than the drift current. A diode not exposed to light has the following current voltage characteristic:

$$I = |I_{drift}|e^{\frac{qV}{kT}-1} \tag{16}$$

When the diode is exposed to light, the drift current is increased, and the characteristic is changing into:

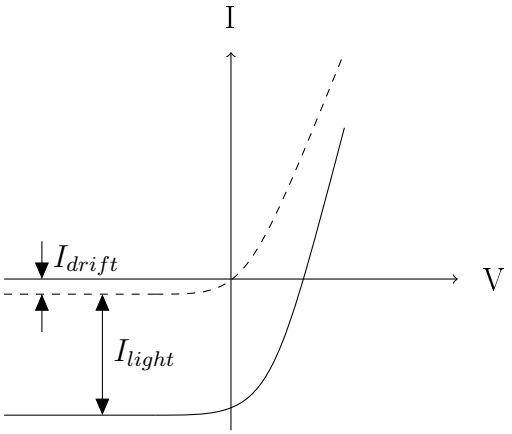

Figure 6: Current-voltage characteristics for a solar cell

For solar cells, the current going out of the cell is usually defined as positive, so that the characteristic is flipped upside-down

$$I = I_{light} - I_{drift}(e^{\frac{qV}{kT}-1}) \tag{17}$$

where I_light, is the current generated by the exposing light. In an open circuit the voltage is defined as

$$V_{OC} = \frac{kT}{q}\ln(\frac{I_{light}}{I_{drift}} + 1) \tag{18}$$

and max power defined as

$$P_m = I_m V_m \tag{19}$$

where P_m is maximum power, I_m is maximum current and V_m is maximum voltage. Solar cell efficiency is defined as

$$\eta = \frac{P_m}{P_{inn}} = FF\frac{I_{belysning}V_{OC}}{P_{inn}} \tag{20}$$

where FF is the fill factor give by

$$FF = \frac{I_m V_m}{I_{light}V_{OC}} \tag{21}$$

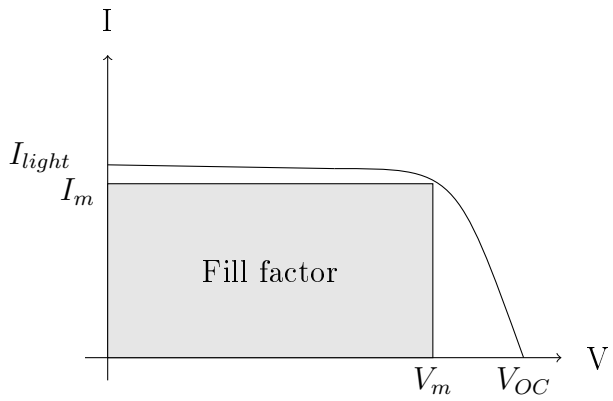

Figure 7: Current-voltage characteristics with fill factor

Solar cells with defects, have a less efficiency than clean samples

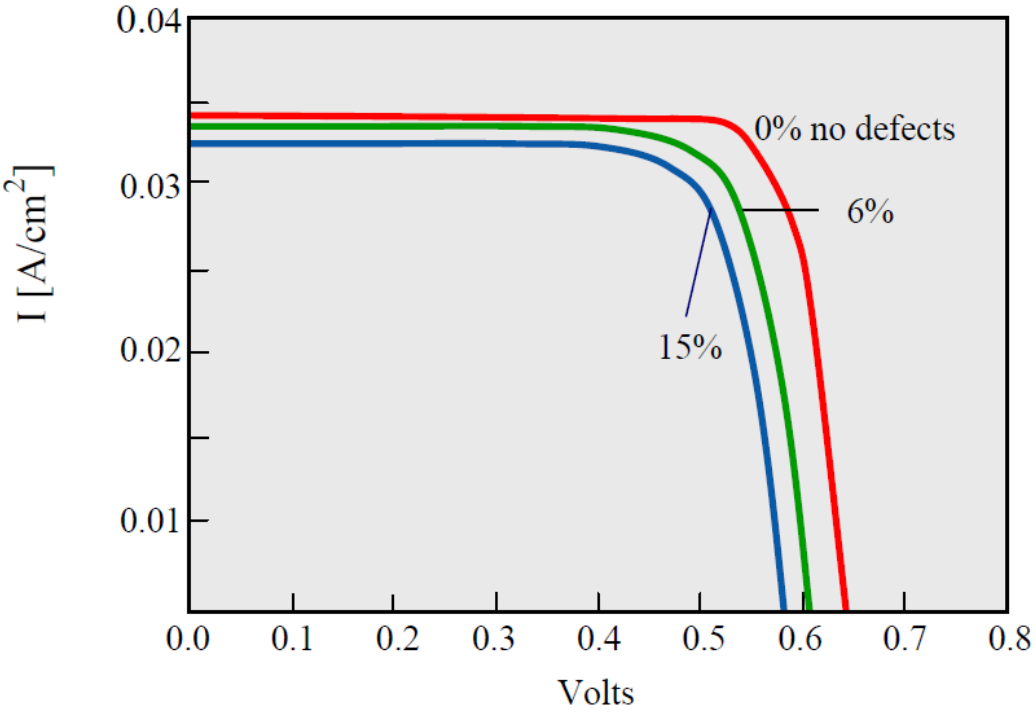

Figure 8: A comparison of calculated I-V characteristics of three cells with 0%, 6%, and 15% of area covered by defects from [3].

which makes it important to be able to characterize defects as well as impurities in order to increase solar cell efficiency.

1.6 Dislocation photoluminescence

Several investigations have documented that dislocations in silicon give rise to characteristic photoluminescence (PL) spectra below the band edge. First showed in [4] which labeled them D1 (0.812eV), D2 (0.875eV), D3 (0.934eV) and D4 (1.000eV). The samples where deformed at 850° C by bending, so that dislocation densities was inhomogeneous along the samples. [4] states that the intensity of theese lines increase closer to the dislocation-rich parts of the crystal. At the same time the intensity of the intrinsic characteristics decrease. The distance between D1-D4 (62 ± 3 meV) corresponds to the energy of the optical phonons in silicon [4]. [4] reports that D1 and D2 are dominant in heavily deformed Si crystals, while D3 and D4 predominate in weakly deformed Si. A similar result was also reported by recent study [5] for small angle grain boundaries using cathodoluminescence.

It has been suggested in [6] that D1-D4 are due to dislocations which have been frozen in under low-shear stress. [6] state that photoluminescence under uniaxial stress shows that D1/D2 originate in the tetragonal defect with random orientation relative to <100> directions. [6] conclude that D3 and D4 are closely related, whereas the independent D1/D2 centers might be deformation-produced point defects in the strain region of dislocations. D1 and D2 is known to be closely related, as well as D3 and D4, and there have been no reports on the D-line spectrum missing only the D1 line [7].

The origin of D1 and D2 is not clear. It has been argued that they originate in electronic transition at the geometrical kinks on dislocations [8], point defects [6] and impurities [9] and/or from the reaction products of dislocations [10]. On the other hand, D3 and D4 lines is generally thought to be related to electronic transition within dislocation cores [11]. In addition, it has been suggested that the D3 line most likely is a phonon-assisted replica of D4 [11].

New lines D5 and D6 emerge when high-temperature, low-stress deformation is followed by low-temperature, high-stress deformation. [6] propose that line D5 is due to straight dislocations and D6 is due to stacking faults. [6] also suggest that D3/D4 photoluminescence is much more characteristic of the dislocations themselves than the D1/D2 emission lines. [12] state that D5 is correlated with electron-hole recombination at localized centers on separate partial dislocations. After annealing at moderate temperatures (T > 360°C) the new lines merge into D4 [12].

Both [4] and [6] studied plastically deformed silicon made by the Czochralski process (Cz-Si). [13] studied dislocations in multicrystalline silicon (mc-Si) and found similar lines with the entire set of D-lines shifted with around 10meV, presumably due to a strain field. Using a laser annealing technique

[14], introducing dislocations on a Cz-Si wafer, confirm the band location of D1-D4 from [6] in [13]. A principal difference between dislocation D'-lines in mc-Si versus D-lines in Cz-Si is a substantial broadening (60-70meV at 77K) of the D1'/D2' lines [13].

Cz-Si [4]	D1	D2	D3	D4
	0.812eV	0.875eV	0.934eV	1.000eV
mc-Si [13]	D1'	D2'	D3'	D4'
	0.80eV	0.89eV	0.95eV	1.00eV

Table 1: Energy positions of dislocation D-lines in Cz-Si and D' bands in mc-Si

[13] reveal a linear dependence of the band-to-band photoluminescence intensity and minority carrier lifetime across entire multicrystalline-Si wafers. Photoluminescence mapping in [13] of the 0.78eV (0.8eV) band intensity reveal a linkage to areas of a high dislocation density. This band should also be visible in room temperature [13].

Dislocation related lines (D-lines) has been observed in low temperature photoluminescence spectra from the regions which included the intragrain defects. [7] concluded that grain boundaries are not active recombination centers. [7] also show a TO-phonon replica of the boron bound exiton at 1.093eV. Intensity of boron bound exciton from the long lifetime regions was higher than that from the short lifetime regions. D-lines reported by [6] are in a short lifetime region. For a long lifetime region, [7] observe a peak at 1.00eV which is not the D4 line, but the zone center optical phonon sideband of the two-hole transition in the boron bound exiton [15].

It is believed that the intra-grain defects observed in the photoluminescence mapping are dislocations decorated with the heavy metals [7]. [16] found that if the contamination level is too low, or too high (dislocation decorated by metal silicate precipitates) the defect photoluminescence band vanished in room temperature. However, a relatively low contamination level of dislocations, in the order of 10 impurity atoms per micron of the dislocation length produces distinguishable defect band luminescence [16].

[17] conclude that defects are metal contaminated dislocation clusters which originated from small angle grain boundaries. [17] study origins of the defects by low temperature photoluminescence spectroscopy, electron backscatter diffraction pattern measurement and the etch-pit observation. [18] demonstrate three areas of a sample with only D3 and D4 present, and conclude that this is due low concentration of metallic impurities.

1.7 Impurities

Diffusion of transition metals into silicon crystals result in a variety of different electrically active levels in the forbidden bandgap. Impurities is also known to create precipitates inside a silicon crystal, which change the photoluminescence spectra compared to interstitial impurities.

There are several units of impurities in silicon that's commonly used. Examples are: ppbw (Parts Per Billion by Weight), ppba (Parts per Billion Atomic) and atoms/cm^3. To convert from ppbw to atoms/cm^3, the following equation can be used:

$$atoms/cm^{-}3 = \frac{10^{-}9\ [ppbw] \cdot N_A \cdot [density(Si)]}{[atomicmassofelement]} \tag{22}$$

where N_A is Avogadro's number, density(Si) is in g/cm^3, and atomic mass is in g/mole. To convert from ppba to ppbw:

$$ppbw = \frac{[atomicmassofelement]}{[atomicmassofSi]} \tag{23}$$

1.7.1 Atom impurities

Early work done by [15] compare intrinsic silicon from the Czochralski process with doped silicon. [15] do extensive photoluminescence study with doping atoms As, P, Sb, Bi, B, Ga, In and Al. The high intensity transverse optical lines occur at 1.0907eV, 1.0916eV, 1.0921eV, 1.0888eV, 1.0924eV, 1.0914eV, 1.0835eV and 1.092eV respectively with the different doping atoms present. Impurities like carbon complexes with many impurities in silicon, resulting in a large variety of photoluminescence centers. Detected complexes are another C atom, one oxygen atom, one N atom, one Ga atom, the four-lithium atom complex, beryllium and numerous radiation damage centers, especially involving oxygen [19]. See appendix 5 for energies.

Doping atoms give rise to different characteristics in the photoluminescence spectra as well. Boron doping exhibits a line right below the silicon bandgap. That particular peak is hard to detect due to a strong luminescence from the silicon itself, but its phonon replicas can be identified (figure 44). Phosphorous doping give rise to a line just below the boron line (figure 45).

Some impurities does not result in any specific photoluminescence spectra, like interstitial chromium [20]. Atleast not for wavelengths up to 1800nm. However, chromium bound with a boron atom can be identified as a peak around 0.85eV where the intensity increase linearly with laser power [20, 21]. Photoluminescence from another impurity, titanium, has been observed

around 2.85eV in 4H silicon carbide by [22], and in 6H by [23] at 2.79eV, 2.82eV and 2.86eV named ABC lines (figure 49). These energies are far beyond that of the silicon bandgap, and can in cases described above, be uniquely identified.

Many of the other identified impurities are located just below the silicon bandgap in the photoluminescence spectra. Spectra for a silicon sample with a low amount of impurities can be seen in figure 43. Copper doping of silicon crystals results in an intense emission at 1.014eV [24]. [12] study Cu doped Si and also observe a shoulder on the D1 line which presumably arises from Cu precipitates at the dislocation.

Another important impurity is iron. [25] observe a spectrum of 0.735eV, which relate to a complex defect containing iron. Here the sample was introduced with Fe atoms into a float-zone silicon crystal (PL at figure 46). An earlier study [26], observe a luminescence spectra around 1.07eV in boron-doped, iron-diffused crystalline silicon and suggest the source is Fe-B pairs. Interstitial iron Fe, is about 10 times more effective as a recombination center than Fe-B pairs by low-level lifetime measurements and therefore reduces the minority carrier diffusion length more strongly (PL at figure 47) [27].

Recent work in [28] show that micro-photoluminescence is an excellent tool for identifying metal precipitates in silicon as seen in figure 9. Iron images in [29] reveal internal gettering of iron to grain boundaries and dislocated regions during ingot growth. The minimum size for detection is 1μm, or even smaller, since the photoluminescence signal might be broadened. Precipitates from Fe and Cu are detected due to reduced band to band recombination intensity. Iron in silicon also affect the defect photoluminescence [28].

1.7.2 Interaction with dislocations

Investigation in [30] show that transition-metal contamination plays an important role in the production of D-band luminescence from silicon samples containing either epitaxial stacking faults or oxidation-induced stacking faults. [14] found that Cu doping resulted in reduced intensity of D1 and D2, and the intensity of D3 and D4 become very small. [12] demonstrate that a complete passivation of the D-band luminescence is achieved at higher Cu and Fe concentration when deliberately contaminating high purity silicon samples which contain dislocations. However impurities like Ni, lead to no detectable changes in the spectrum [12]. D-band recombination in Si is found to be independent of impurities trapped at dislocations [12], and [10] concluded that metallic impurities don't seem to be related to D1 and D2 luminescence. Even so, it is still generally accepted that metal impurity influence

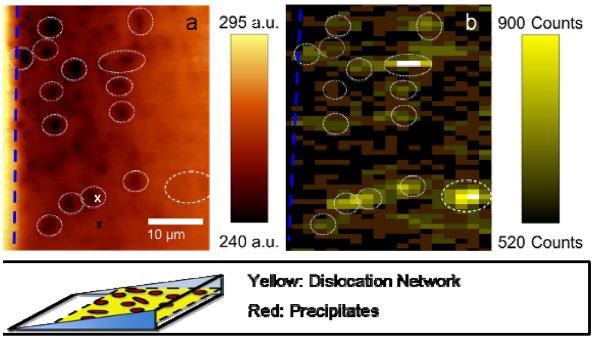

Figure 9: Bottom: Scheme of the sample preparation with the polished angle. Top: A Intensity of the BB PL peak at room temperature (a), and of the iron X-ray Kα fluorecence (b) from [28]. The dislocation network intersects the surface to the right of the dashed blue line. The white circles show recombination active precipitates.

it. Metal precipitation at crystal defects during the crystal growth can clean grains from impurities, and thus improve the performance as suggested for iron in [31]. A recent example of interaction with defects is iron precipitates in [28], showing an enhanced defect photoluminescence at 1.3μm (0.95eV). The same study show that copper contamination almost completely suppress the defect photoluminescence. This is in agreement with [14]. Supression of defect photoluminescence by high copper concentrations was also reported in [32]. Cu precipitates can be located by reduced intensity of the band to band photoluminescence peak, both in areas with dislocations, and without [28].

Electron hole droplets (EHD), free excitons (FE) and bound excitons (BE) localized on phosphorus atoms has been steadily observed in [33] with photoluminescence on samples with low-dislocated regions. When increasing dislocation density the FE, BE and EHD bands decrease sharply. This may be due exciton capture by dislocation lines D1,D2 and non-radiative recombination [33]. EHD photoluminescence intensity is highly dependent on the pumping power [34]. There is a linear dependence, and pumping with 3mW or less makes it hardly visible in [34].

D1 line is shifted towards higher energies under uniaxial elastic deformation of samples with introduced dislocations or after their annealing in oxygen at 750°C [35]. Room temperature mapping of the 0.77eV band is attributed to oxygen precipitates in in thermally treated silicon made by the Czochralski process (Cz-Si) [36]. The increase of this band on the dislocation lines is due to the preferential precipitation of oxygen [36]. Later, [37] state

that the deep-level emission from multicrystalline silicon with an intensity maximum at 0.78eV at room temperature is different from that of the D1 line at low temperature. Furthermore, [37] suggest that the 0.78eV emission is associated with oxygen precipitation, and that the intra-grain defects are dislocation clusters decorated with oxygen impurities in addition to heavy-metal impurities. [38] state that the origin of trap densities in multicrystalline silicon could be structural crystal defects, which are highly decorated with oxygen precipitates.

2 Experimental

2.1 Samples

Name	Description	Feedstock
R6-Q3-210	Polysilicon, electronic grade, clean feedstock	Siemens process
ES1-Q3-201	Large amount of P and B, solar grade, dirty feedstock	From Elkem [39]
MH2-Q3-201	Same as ES1 with added Cr, solar grade, dirty feedstock	From Elkem [39]

Table 2: Samples

2.1.1 R6-Q3-201

This sample is from a clean feedstock, with low amount of impurities. B,Al and Fe where measured by Glow-Discharge Mass Spectrometry (GDMS), O and C where measured by Fourier transform infrared spectroscopy (FTIR).

Impurity	ppbw	atoms/cm^3
B	112.01	$1.45 \cdot 10^{16}$
Al	19.48	$1.0 \cdot 1010^{15}$
Fe	nd	nd
C	2576	$2.26 \cdot 10^{17}$
O	1932	$8.87 \cdot 10^{16}$

Table 3: Impurities in R6

The impurities that are not listed were not analyzed, and are expected to be present in very low levels (tenths of ppbw).

2.1.2 ES1-Q3-201

This is a regular solar grade sample which originate from a compensated feedstock from Elkem Solar, from 90% ingot height. It has been Sopori etched to bring out dislocations [40].

Boron contaminants appear to be between 550 and 700 ppbw, which is between $7.1 \cdot 10^{16}$ and $9.7 \cdot 10^{16}$ atoms/cm^3 respectively using 22. Phosphorus is measured around 1200-1500 ppbw, which is 5.4-6.8 $\cdot 10^{16}$ atoms/cm^3. Aluminum contaminants is just below $2.6 \cdot 10^{15}$ atoms/cm^3. Other contaminants like Ti and Fe have very low values: less than $1.2 \cdot 10^{14}$ and

$3.8 \cdot 10^{14}$ atoms/cm^3 respectively. For the lighter atom impurities, O have $1.7 \cdot 10^{17}$ atoms/cm^3 and C have $6 * 10^{17}$ atoms/cm^3 [39].

2.1.3 MH2-Q3-201

This sample is almost identical to ES1, but the sample also have extra chromium added. Chromium contaminants appear to be between 2 and 5 ppbw [39] which corresponds to $5.4 \cdot 10^{13}$ and $1.3 \cdot 10^{14}$ atoms/cm^3 respectively using 22, but exact concentration might be a little lower due detection limit of the instrument.

2.2 Setup

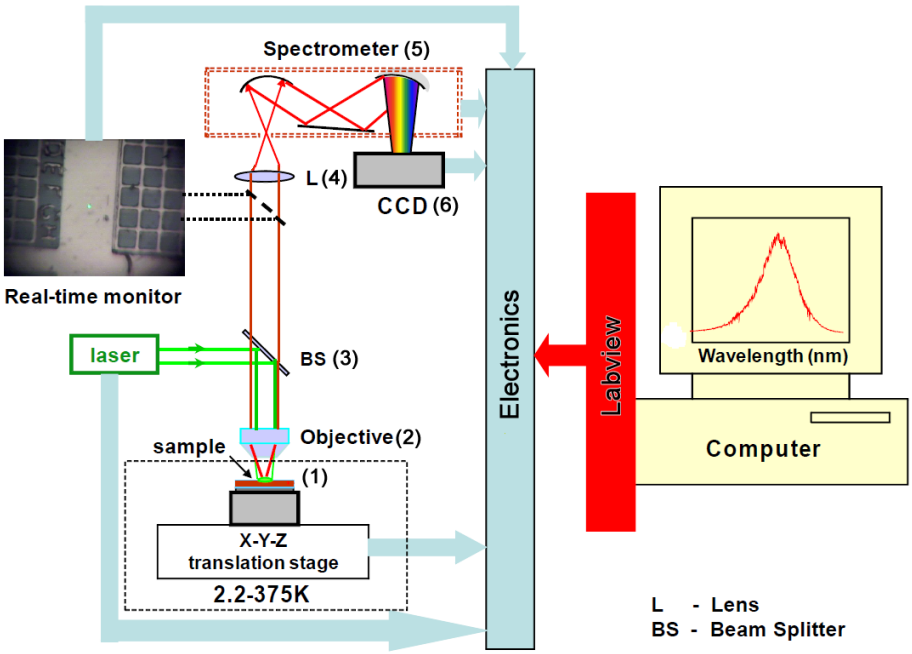

Figure 10: Lab setup

#	Part	Product #	Manufacturer
1	Cryostat	Janis ST-500	Janis Research Company
2	Objective	NT56-982	Edmund Optics
3	Beam splitter	BS017	Thorlabs
4	Lens	ACN127-020-B	Thorlabs
5	Spectrometer	iHR550 Imaging Spectrometer	Horiba Scientific
9	Camera	InGaAs Spectroscopy CCD	Andor Technology

Table 4: Lab setup optical components

2.3 Pumping wavelength

Pumping light needs to have enough energy to fill all available states in the crystal lattice, in order to detect defects and impurities. For silicon, which has a bandgap of around 1.1eV, has most impurity/defect bands below the bandgap. In order to fill these states, the pumping wavelength should be below 1125nm, which corresponds to energies just over 1.1eV.

Silicon has different absorption lengths for different wavelengths. For 1125nm, the absorption depth is nearly 200 μm [41]. Compared to absorption for 532nm, 1125nm reach 200 times deeper into the sample.

Absorption length of about 1 μm for 532 nm laser, means that iron precipitates deeper in the sample won't be detected [28]. This limitation might be overcome by an excitation laser with a longer wavelength and absorption length in silicon. [5] report that small angle grain boundaries in multicrystalline silicon of 1°-1.5° show D3 and D4 lines, while 2°-2.5° show D1 and D2 lines. Comparing to data from electron beam induced current measurements show D1 and D2 lines to be correlated with shallow levels, while D3 and D4 appear in both shallow and deep levels [5].

A pumping wavelength of 800 nm is chosen for excitation. This corresponds to an absorption depth of 12 μm in silicon. With a larger wavelength, it would be invisible to the naked eye, and make it much more difficult to align the setup, and make sure nothing is blocking the pathway. In the case of an imperfect filter in front of the spectrometer, 800nm (1.55eV) and the second order diffraction maxima at 1600 nm (0.775 eV) would be outside the most interesting wavelengths from silicon luminescence (see table 5).

2.4 Spot size

Having a small diameter on the pumping laser allows for a high resolution of characteristics on the sample. In an iron contaminated sample, [28] show

that at some distinct spots of a size between 1μm and 4μm, the band to band photoluminescence peak is particular low at spots with iron precipitates.

A large electron hole droplet could overshadow characteristics from impurities in the sample. [34] show that electron hole droplets become more intense for a smaller volume, with a silicon nanolayer smaller than the absorption depth of the laser. [34] used a 488nm pumping laser with 1,5μm diameter, on silicon nanolayer thickness of 50nm and 340nm. For the 50nm layer, [34] observed a large electron hole droplet, even for small pumping intensities, with the same amount of photo excited carriers per volume as for the 340nm layer. Assuming that a small volume give rise to a larger electron hole droplet, it would be a limiting factor for the spot size and pumping wavelength.

For the setup given here, the spot size is around 2 μm.

2.5 Laser intensity

With a large pumping intensity, an electron hole droplet become visible in the specter around 1.08eV in bulk silicon [42]. [34] show that electron hole droplets occur at weak excitations (0.75mW) and even at high temperatures for a silicon nanolayer of 50nm. For thickness of 340nm, the electron hole droplet show up at pumping intensity of 3mW and above, and the intensity of the electron hole droplet grow larger than for the free exciton at 15mW. This electron hole droplet is not wanted, as it can mask characteristic photoluminescence from impurities.

With a larger pumping intensity, the impurity photoluminescence would in some cases also increase. Photoluminescence from chromium bound with a boron atom is known to increase linearly with laser power [20, 21], and would be easier to detect at a higher pumping intensity.

2.6 Expected results

2.6.1 Phosphorus and boron doped samples

With fairly high concentrations of doping atoms, it's expected that they show up as separate lines in the photoluminescence spectra. [15] observe a line around 1.0924eV which is attributed to B^{TO}. Concentrations values for B in [15] are $6 * 10^{16}$ cm^{-3}. Also observed is a phosphorus line at 1.0916eV, with 8*10^{16}cm$^-$3 phosphorus atoms. ES1 and MH2 have similar B and P values, and is expected to show the same behavior. (See figure 44 and 45 in appendix 3.3.4)

There is a photoluminescence line involving carbon bound to oxygen in Czochralski silicon known as the C-O band [19]. In [43], it was observed only in crucible grown silicon, but not in float zone. In the crucible grown silicon, the oxygen impurities where $2 \cdot 10^{18}$ atoms/cm^3, which is over ten times more than in ES1 and MH2. This makes it unlikely that any C-O complex luminescence will be strong enough to be detectable in these samples.

Another line involving carbon, is the two-carbon atom band [19]. This band has been detected in float-zone silicon with C = $9.7 \cdot 10^{16}$ cm^{-3} after irradiation, together with the C-O complex line. The relative intensity between the C-O band and the two-carbon atom band in [19] show that the 969 meV band is close to 5 times larger than the 789 meV band. With both MH2 and ES1 having carbon impurities around $6 \cdot 10^{17}$ cm^{-3} it is possible that this line at 969 meV will be visible.

As for aluminum, [15] show a line at 1.09 eV called Al^{TO} in a sample with $2 \cdot 10^{16}$cm^{-3} Al doping atoms. In ES1 and MH2, the Al impurities are 20 times less. In addtion to a fairly low value of Al impurities, the Al^TO line is very close to the I^{TO}, which can make it difficult to detect, and not likely to show up in the results.

Fe bound with boron is also known to give rise to photoluminescence [26]. The sample used in the article had 10^{13} to 10^{16} cm^{-3} boron doping concentration. The article doesn't mention how many Fe impurity atoms that's introduced into the sample, but it's done by high temperature diffusion, and assumed to be considerably larger than for all the samples in this study.

Based on the low values of Fe impurities in these samples, it's assumed that interstitial Fe won't have any effect on the photoluminescence bands. The same goes for Ti, which also have a very low amount present.

2.6.2 Sample with added Chromium

This sample have the same impurity values as ES1, except for chromium. The closest comparison is samples used in [20]. Here, luminescence spectra was observed for chromium in an p-type sample. Interstitial chromium concentrations where between 10^14 and $10^16 atoms/cm^-3$ in [20].

Chromium in an n-type sample doped with phosphorus atoms does not result in any luminescence, but chromium bound with boron show a clear line at 0.8432eV (CrB^0). The reaction velocity for the formation of CrB pairs at room temperature depend on the boron concentration. For large (10^15cm$^-3$) boron content, the chromium-boron reaction reach saturation in less than a day after chromium diffusion [20].

MH2 are neither n og p-type, however there is enough boron atoms to

saturate chromium by forming CrB pairs. Chromium atoms are in the order of 10^{14} atoms/cm^3 which is similar to that in [20]. Expected photoluminescence spectra is therefor expected to be similar. (See figure 48 in appendix). With most of the boron bound with chromium, it is likely that the boron lines will be severely reduced compared to ES1, and not detectable. There are also Fe impurities present in the sample, that can form bonds with boron. Based on the low amount of Fe in this sample, those bonds are not believed to have any impact on the photoluminescence.

2.6.3 Sample from clean feedstock

Having carbon values around $2.26 \cdot 10^{17}$, it is possible that the two-carbon atom band is visible here also. Else this sample is expected to only show intrinsic values similar to [15] in so called "'good"' areas due to low concentration of impurities. However, there might be precipitates and higher concentration of impurities at the grain boundaries and dislocations. Particularly heavy metals like Fe and Al can be detected here. It is expected that the band to band recombination from silicon show considerably lower intensity for these areas.

2.7 Results plotting

In order to plot the results from the spectrometer, there are a few manipulations that's needed.

2.7.1 Disregarding defect pixels

By taking a spectra with the shutter closed, it is possible to measure the dark current coming from the camera. The dark current should be equally distributed across the pixels, based on the assumption that all pixels behave the same. For long integration time, this is not the case:

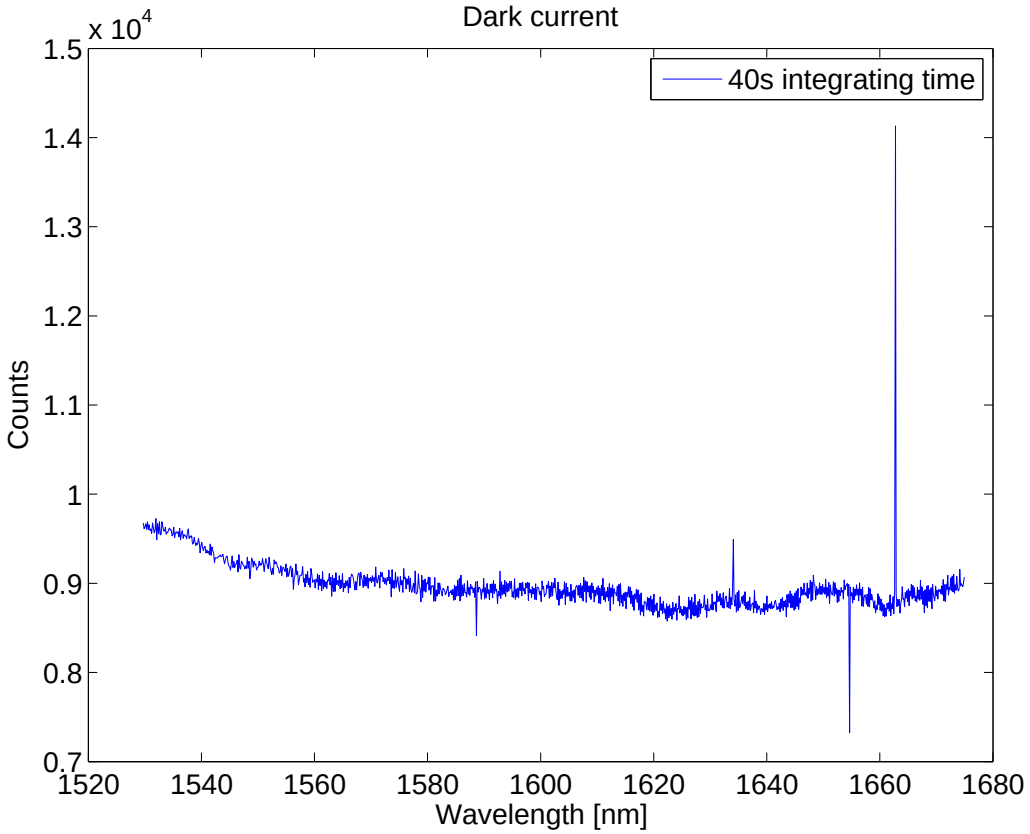

Figure 11: Dark current signal from the camera with defective pixels with shutter closed, and CCD at -75°C using a random center wavelength

To solve this problem, the four pixels are disregarded, and the value of the neighbor pixel has been used instead. Matlab code for this is available in the appendix. Comparing the before and after clearly show how this is done:

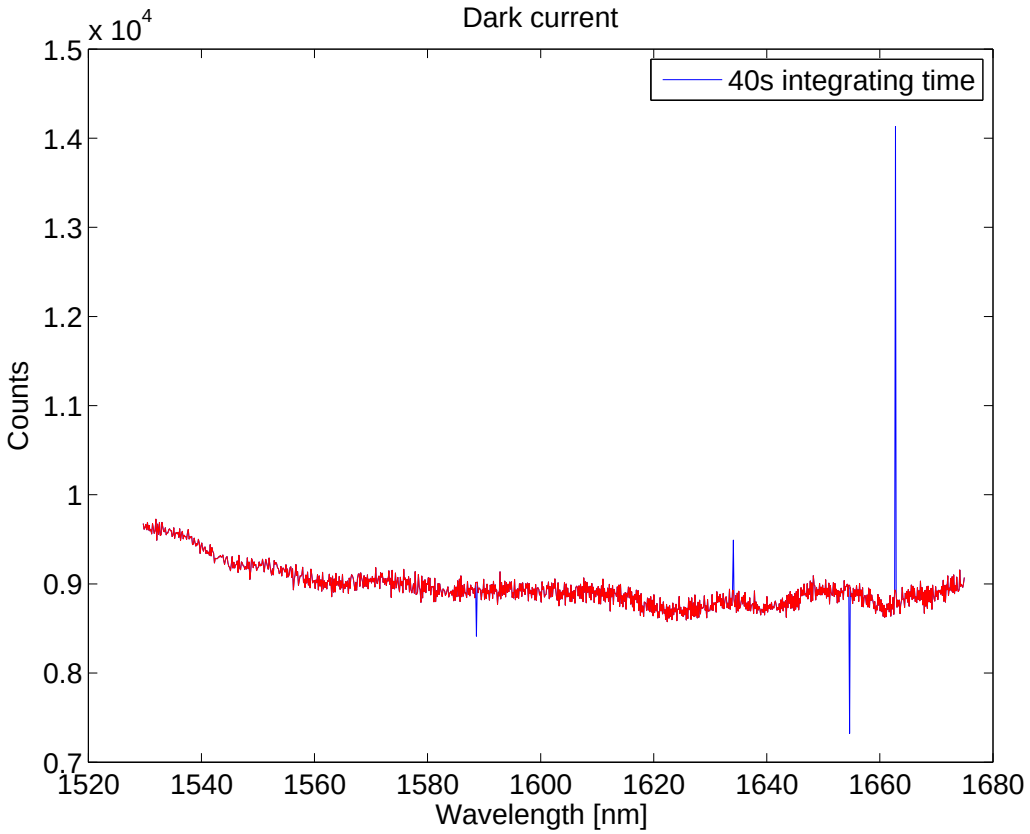

Figure 12: Dark current signal from the camera with defective pixel correction in red using a random center wavelength

The defective pixels are less apparent for shorter integration time, but still a problem:

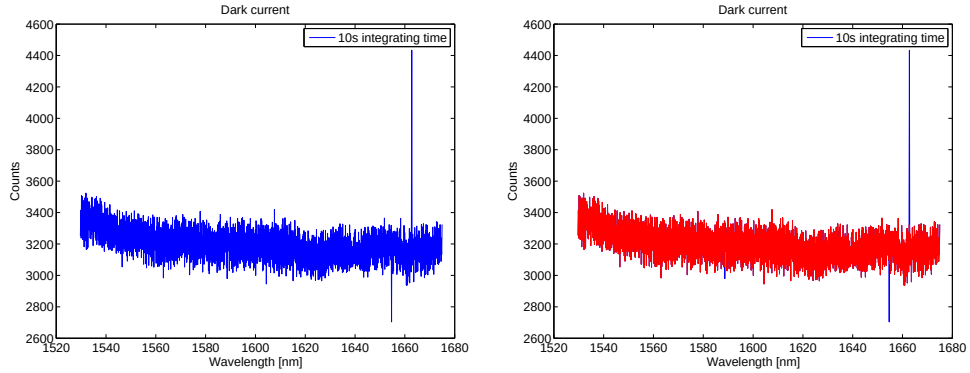

(a) Dark current without correction (b) Dark current with correction (red)

Figure 13: Dark current with 10s integration time using a random center wavelength

Dead pixel correction is performed in all results.

2.7.2 Noise reduction

As seen in the previous section, there is a dark current signal present. Ideally, all pixels should behave exactly the same, and give an exact dark current offset to subtract. This is not the case. The dark current is unevenly distributed over the pixel array, and needs to be measured by itself in order to remove it. The dark current noise shape is fairly static, with some white noise elements on top, but the shape is nearly identical from one measurement to the other with the CCD at a constant temperature.

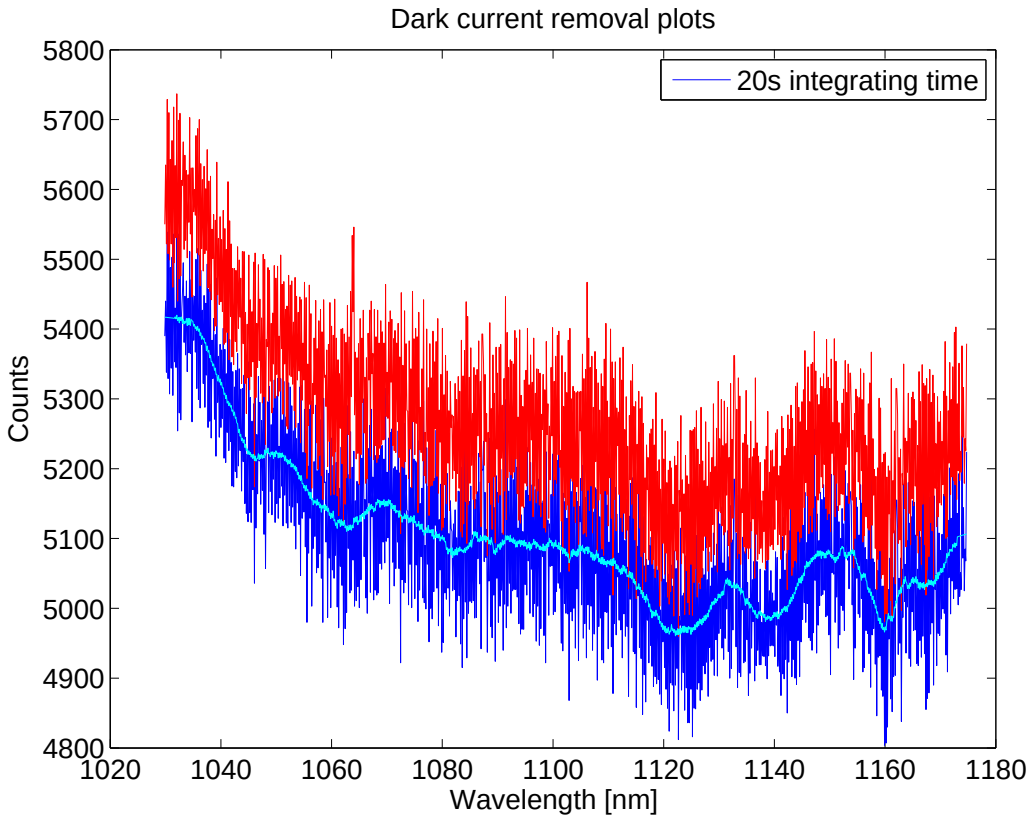

Figure 14: Dark current (blue) and dark current + background noise (red) with filtered noise floor estimation (cyan)

By subtracting the offset found in the dark current noise measurement, only background noise should be present. The matlab code used to do this can be found in the appendix.

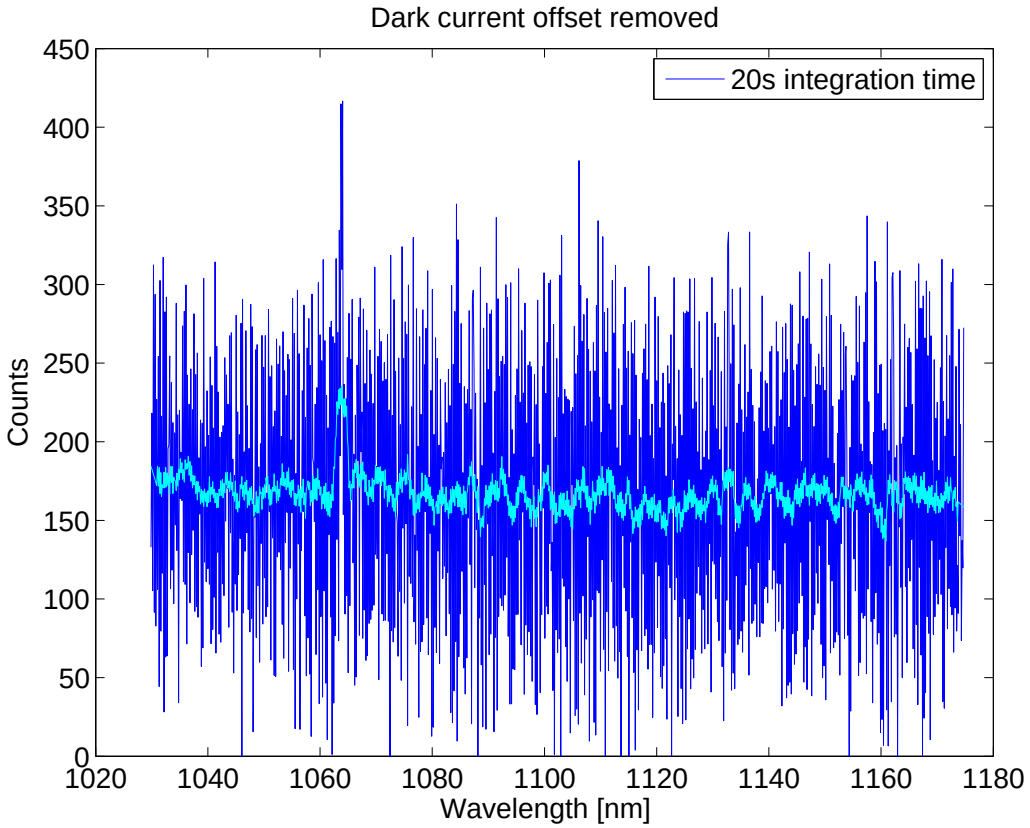

Figure 15: Dark current removed from background noise (blue), and filtered signal (cyan)

It appears that the dark current noise is larger with the shutter open, compared to closed. But a more critical noise in the spectrum is a background signal around 1064nm. The spectrometer has a range of 140nm when using 300 as grating. It has proven difficult to align the system so that the entire array of pixels in the camera get an equally distributed light beam. And based on the noise level, the nm interval is chosen as 100nm, in order to remove the left hand side of the spectra when gluing different intervals together. This also avoid the problem of not hitting the entire array evenly. To get a full overview over the background noise, a full spectra was done, and glued together. This full spectra show that the artifact visible in 15 is the only background noise line visible in the wavelength area 800-1650nm.

3 Results

Results have been corrected for dead pixels, measured dark current, and measured background noise unless otherwise specified. Grating is fixed at 300, and pumping wavelength is 800nm. Counts is a number given from the spectrometer which relate to the relative intensity detected by the pixel in the CCD.

3.1 R6-Q3-210

This is the electronic grade sample, with a very low amount of impurities.

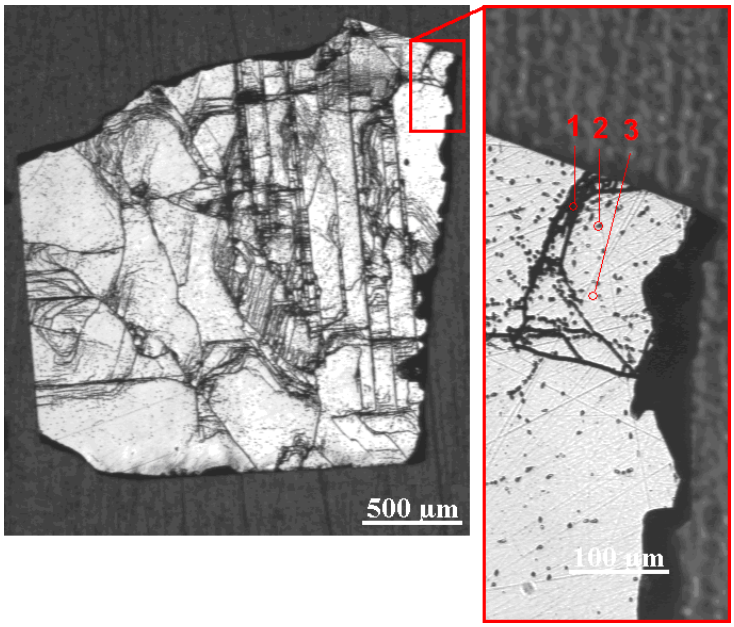

Figure 16: Sample R6-Q3-210 A picture taken using light microscope. Area 1,2 and 3 are spots where photoluminescence has been measured.

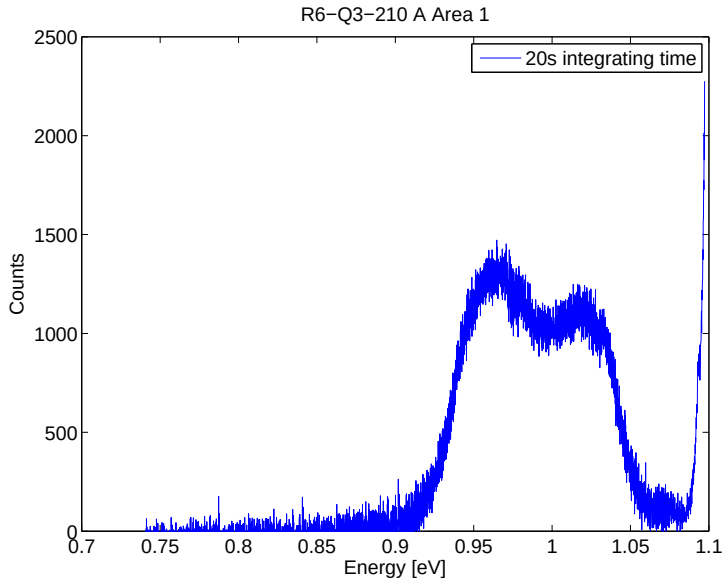

Figure 17: Sample R6-Q3-210 A pumped with 170mW at 10K in a dislocation line (Area 1 in figure 16).

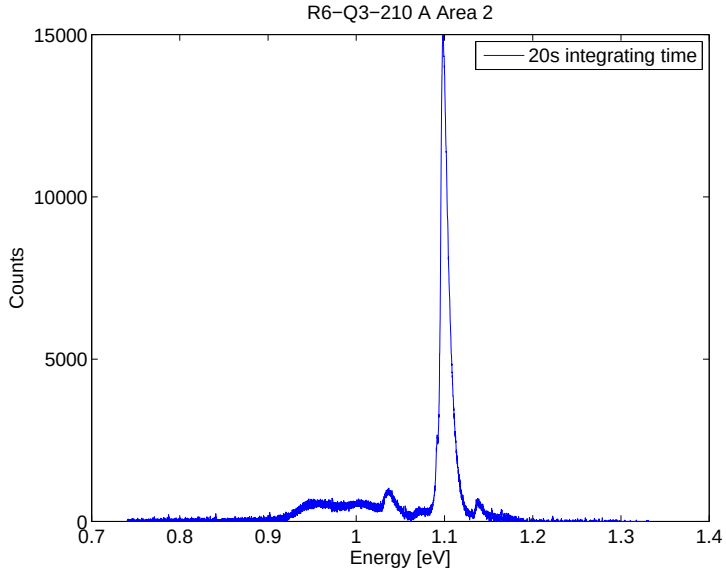

Figure 18: Sample R6-Q3-210 A pumped with 170mW at 10K in a dislocation dot (Area 2 in figure 16).

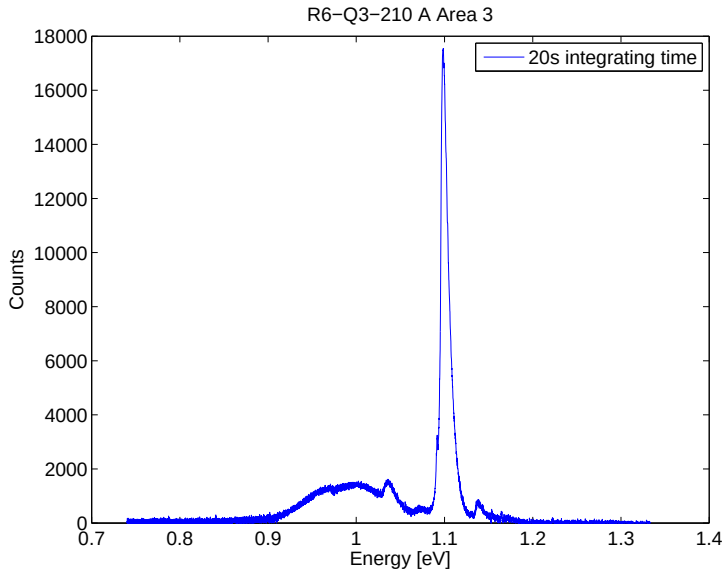

Figure 19: Sample R6-Q3-210 A pumped with 170mW at 10K in a dislocation free area (Area 3 in figure 16).

3.2 ES1-Q3-201

This sample is from a dirty feedstock, with large amount of P and B.

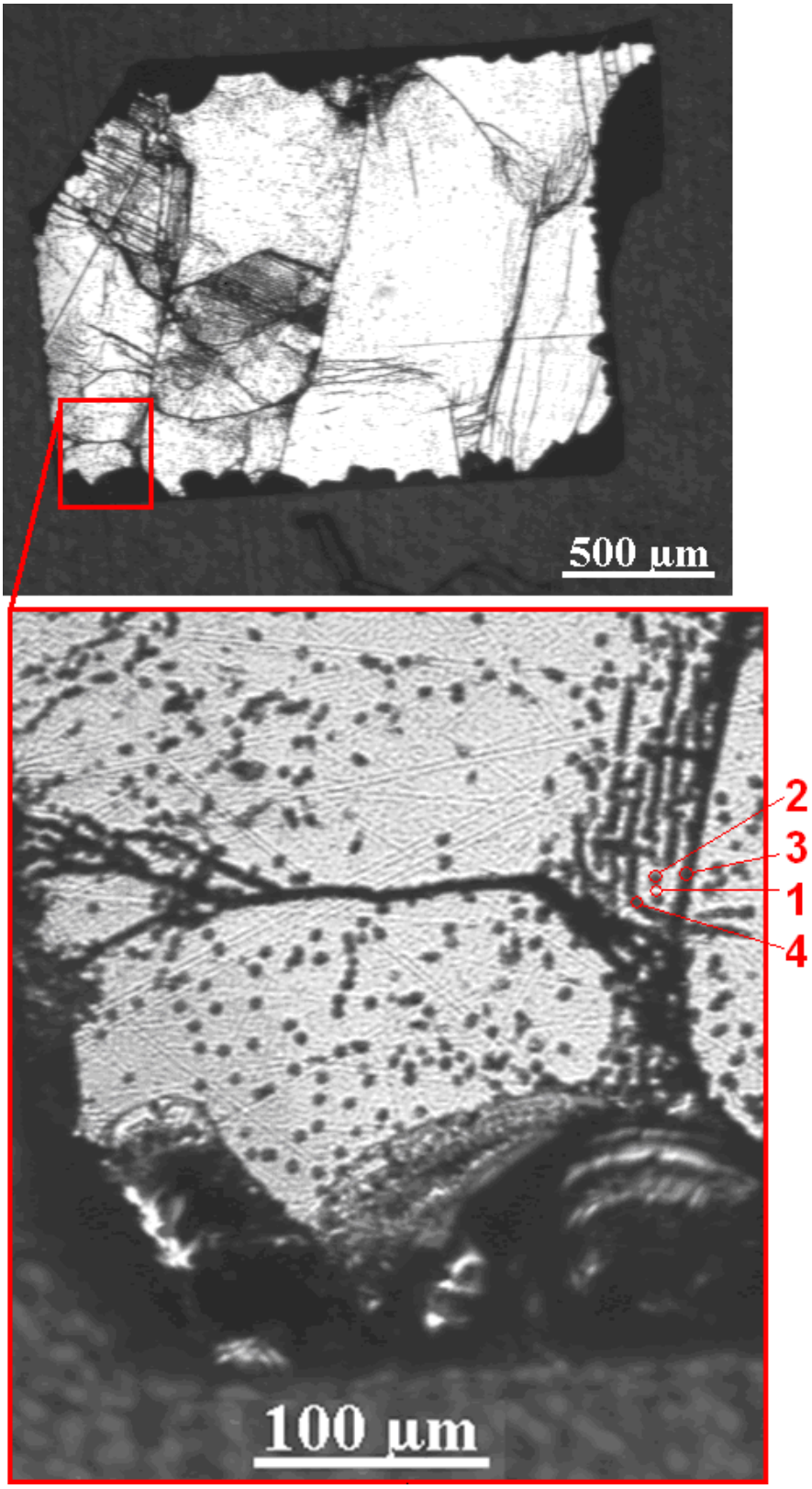

Figure 20: Sample ES1-Q3-201 C 210 Å picture taken using light microscope. Area 1,2,3 and 4 are spots where photoluminescence has been measured.

3.2.1 Room temperature

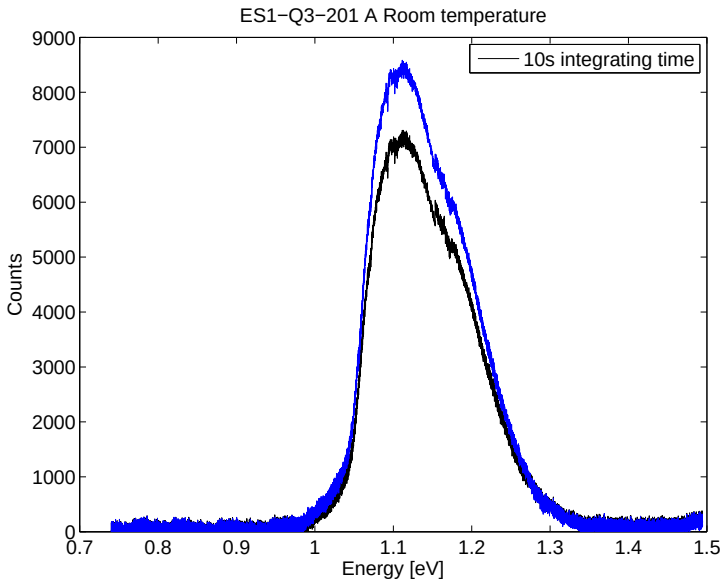

Figure 21: Sample ES1-Q3-201 A pumped with 26mW at 295K in a dislocation line (black) and in a clean area (blue). An estimated dark current offset has been subtracted.

3.2.2 Low temperature

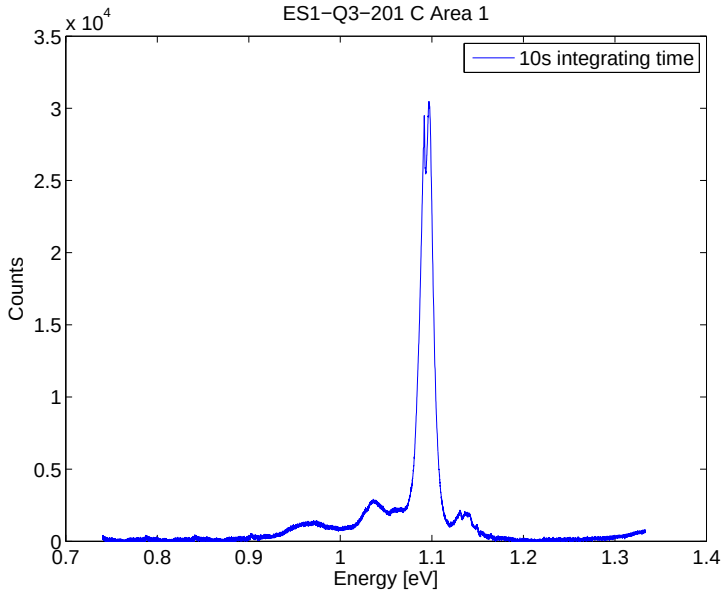

Figure 22: Sample ES1-Q3-201 C pumped with 170mW at 12K in a dislocation free area (Area 1 in figure 20).

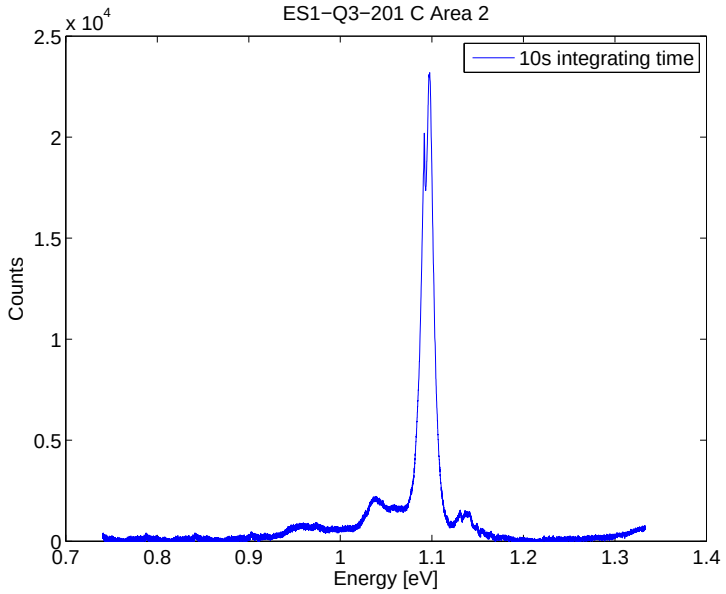

Figure 23: Sample ES1-Q3-201 C pumped with 170mW at 12K in a dislocation spot (Area 2 in figure 20).

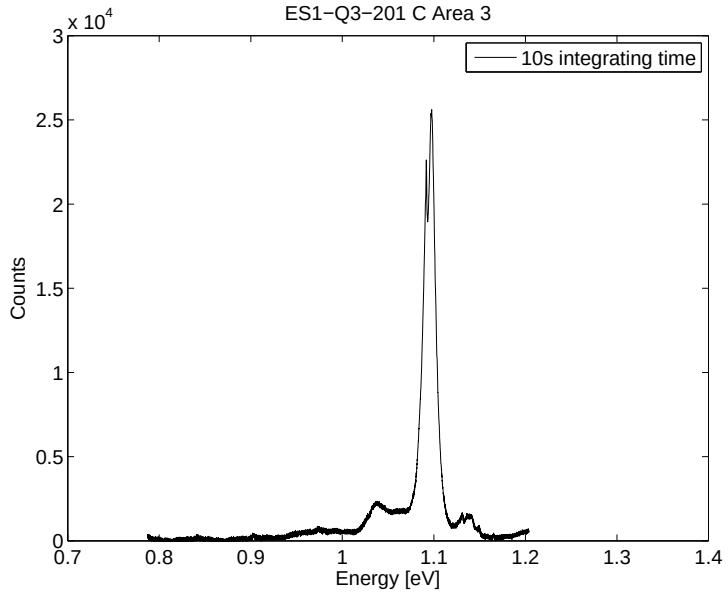

Figure 24: Sample ES1-Q3-201 C pumped with 170mW at 12K in a grain boundary (Area 3 in figure 20).

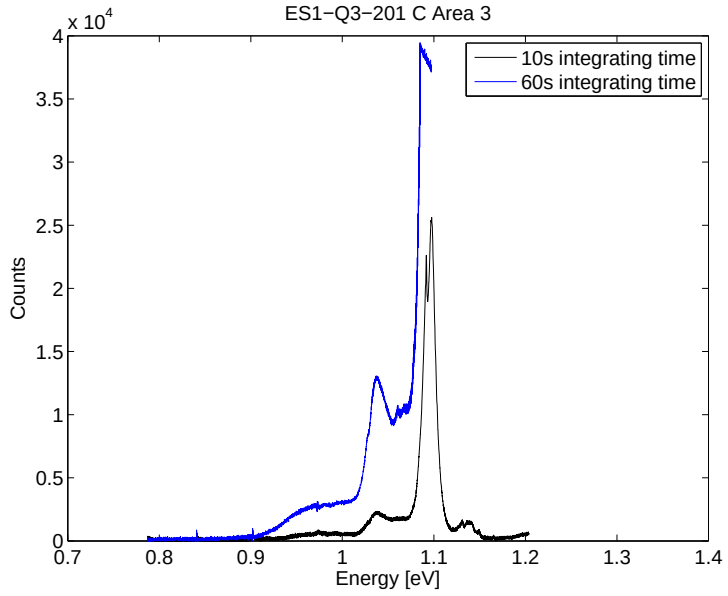

Figure 25: Sample ES1-Q3-201 C pumped with 170mW at 12K in a grain boundary (Area 3 in figure 20) with the result in figure 24 plotted as the black line.

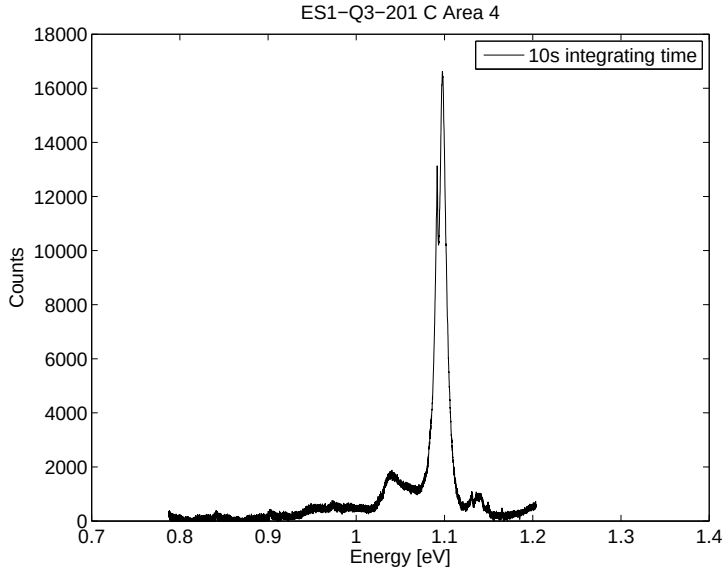

Figure 26: Sample ES1-Q3-201 C pumped with 170mW at 14K in a dislocation line (Area 4 in figure 20).

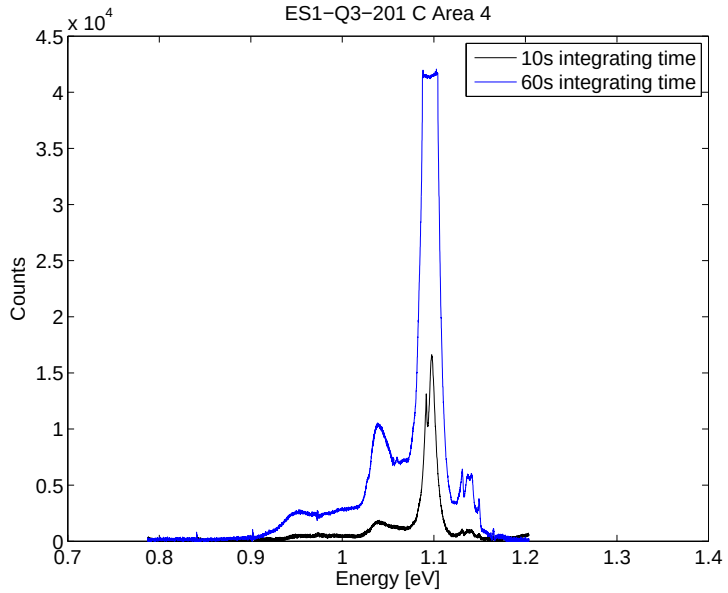

Figure 27: Sample ES1-Q3-201 C pumped with 170mW at 14K in a dislocation line (Area 4 in figure 20) with the result in figure 26 plotted as the black line. For 60s integration, the main TO line around 1.1eV is saturating the camera.

3.3 MH2-Q3-210

This sample is the same as ES1-Q3-201 except for added chromium in this one.

3.3.1 Room temperature

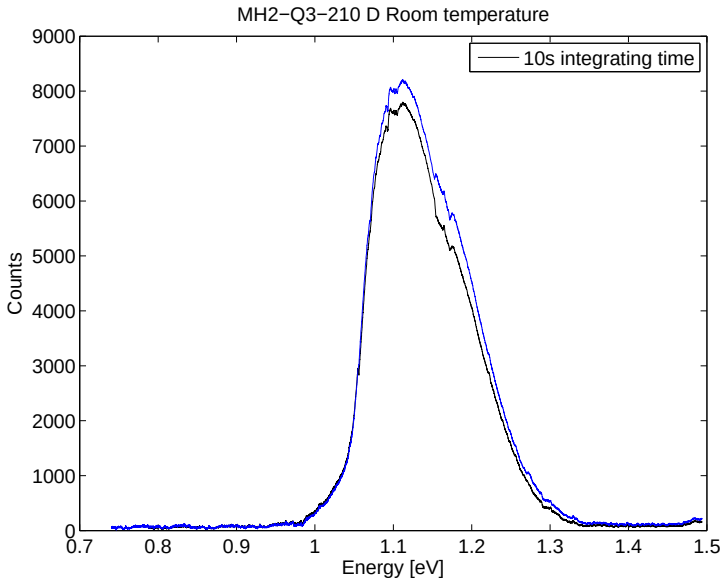

Figure 28: Sample MH2-Q3-210 C pumped with 26mW at 295K in a dislocation free area (blue), and in an area with dislocations (black). An estimated dark current offset has been subtracted, and results are Savitzky-Golay filtered for easier comparison.

3.3.2 At 70K

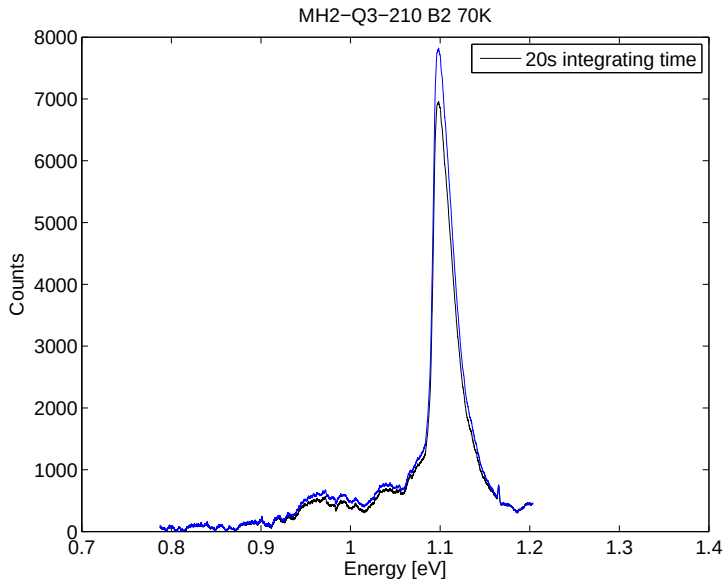

Figure 29: Sample MH2-Q3-210 D pumped with 170mW at 70K in a dislocation free area (blue), and in an area with dislocations (black). An estimated dark current offset has been subtracted, and results are Savitzky-Golay filtered for easier comparison.

3.3.3 Low temperature

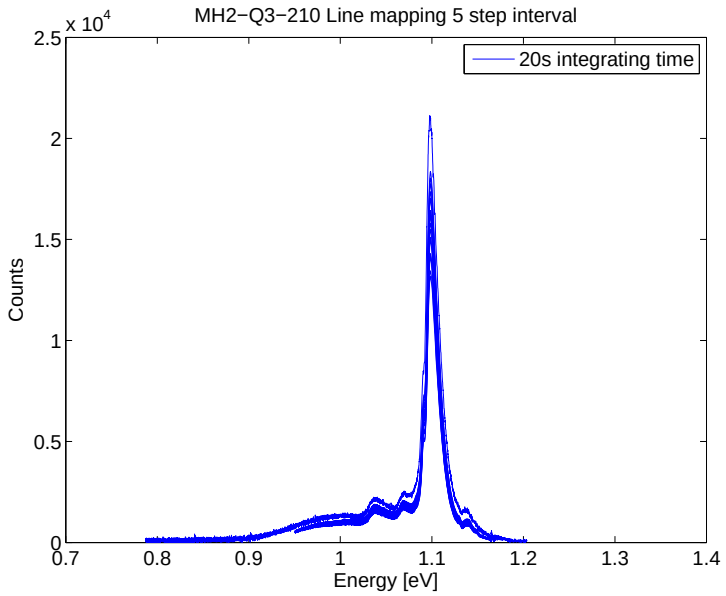

Figure 30: Sample MH2-Q3-210 B2 pumped with 170mW at 12K in a dislocation free area (Area 1).

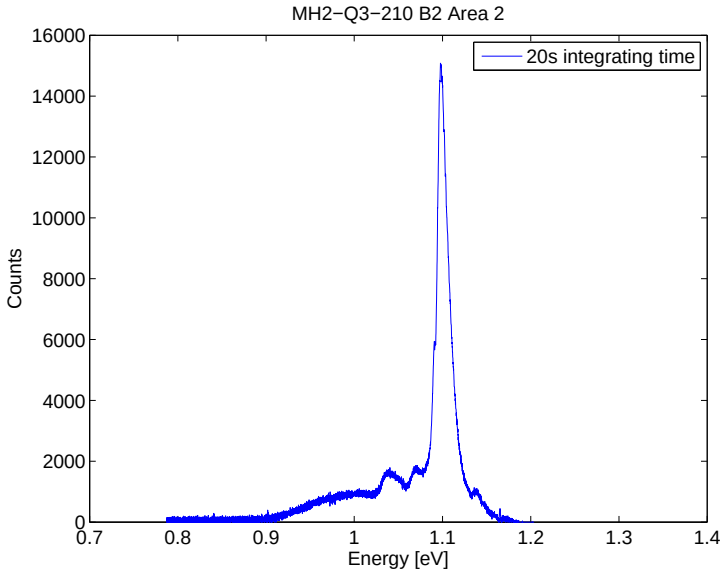

Figure 31: Sample MH2-Q3-210 B2 pumped with 170mW at 12K in a dislocation line (Area 2).

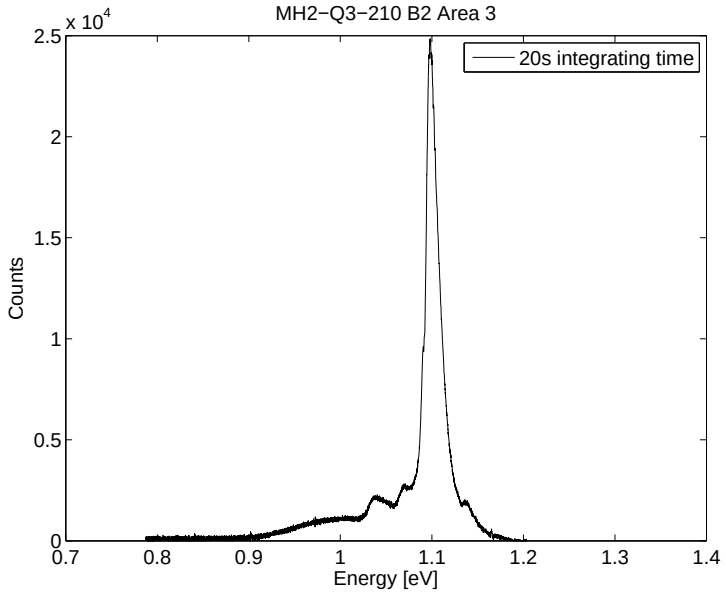

Figure 32: Sample MH2-Q3-210 B2 pumped with 170mW at 12K in a dislocation dot (Area 3).

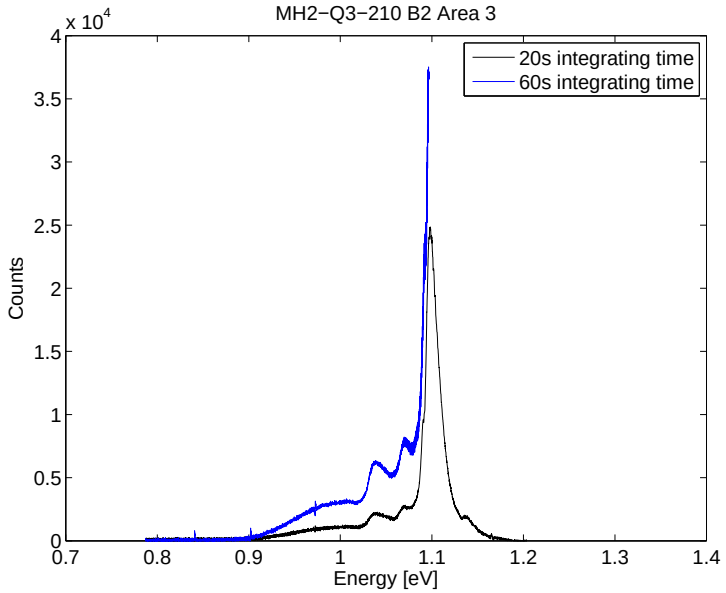

Figure 33: Sample MH2-Q3-210 B2 pumped with 170mW at 12K in a dislocation dot (Area 3) with 20s integration time (black) and 60s integration time (blue). The 60s integration time has an estimated dark current offset subtracted, in addition to measured dark current due to mismatched dark current measurement.

3.3.4 Line mapping

These results are a line mapping of different spots on the sample.

Positions 1-10 has en equally large distance in between them, with position 1 in figure 34 and position 10 in figure 35.

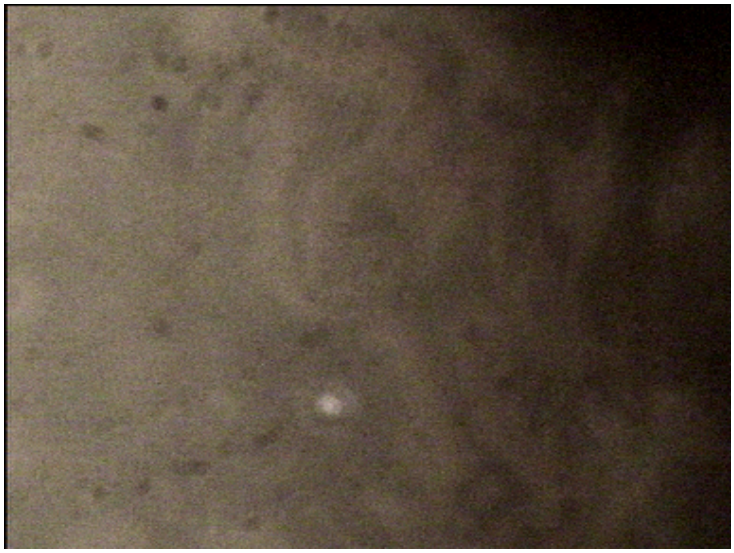

Figure 34: Sample MH2-Q3-210 B2 Line mapping end position. Picture is from the camera inserted into the detection path by use of a flip mirror, and sample illuminated by white light. The bright spot is reflections from the pumping laser.

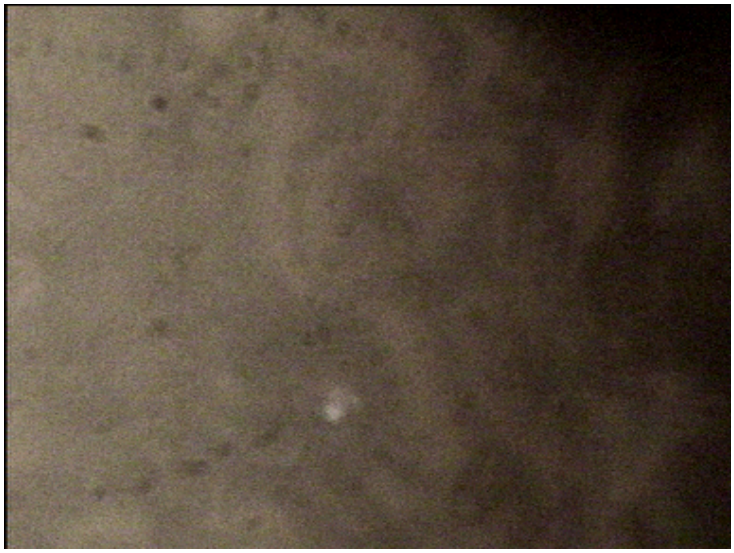

Figure 35: Sample MH2-Q3-210 B2 Line mapping start position. Picture is from the camera inserted into the detection path by use of a flip mirror, and sample illuminated by white light. The bright spot is reflections from the pumping laser.

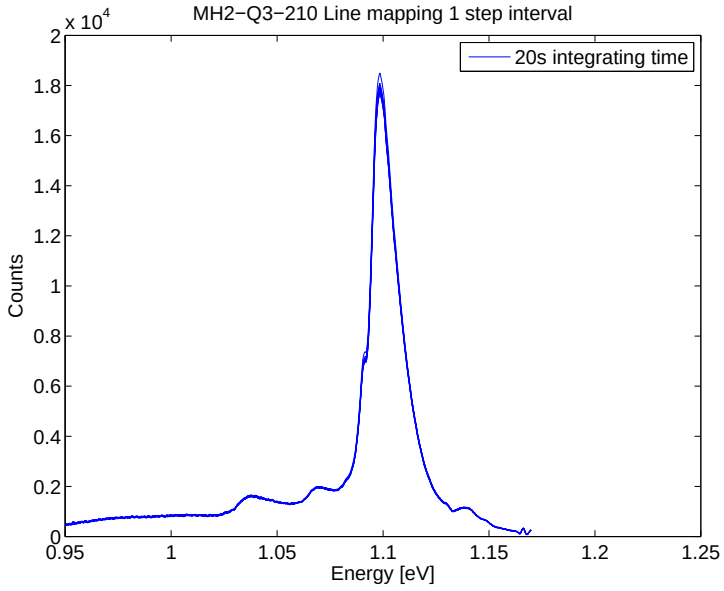

Figure 36: Sample MH2-Q3-210 B2 pumped with 170mW at 14K line map using 10 small steps.

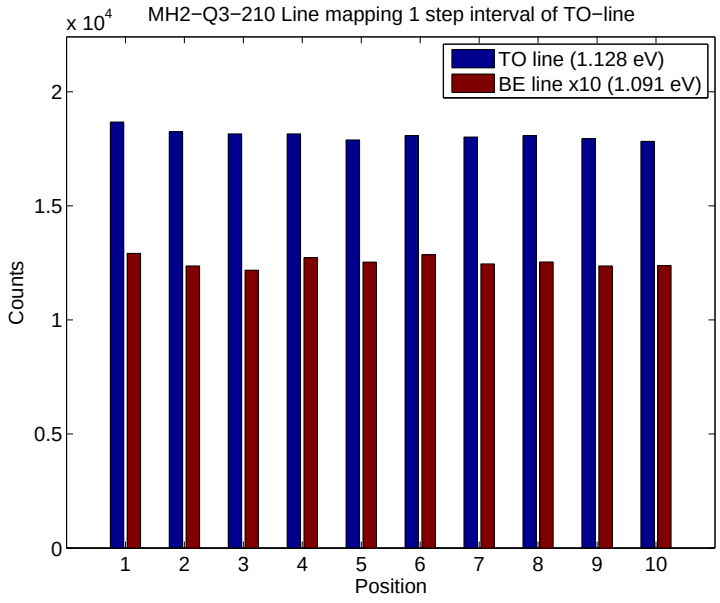

Figure 37: Sample MH2-Q3-210 B2 pumped with 170mW at 14K line map using 10 small steps, looking at TO and BE line only from results in figure 36.

Positions 1-20 has en equally large distance in between them, with position 1 in figure 38 and position 20 in figure 39.

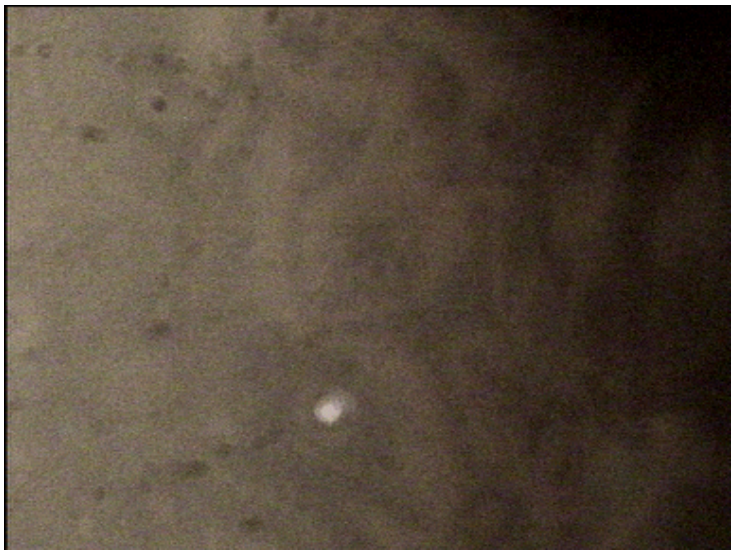

Figure 38: Sample MH2-Q3-210 B2 Line mapping end position. Picture is from the camera inserted into the detection path by use of a flip mirror, and sample illuminated by white light. The bright spot is reflections from the pumping laser.

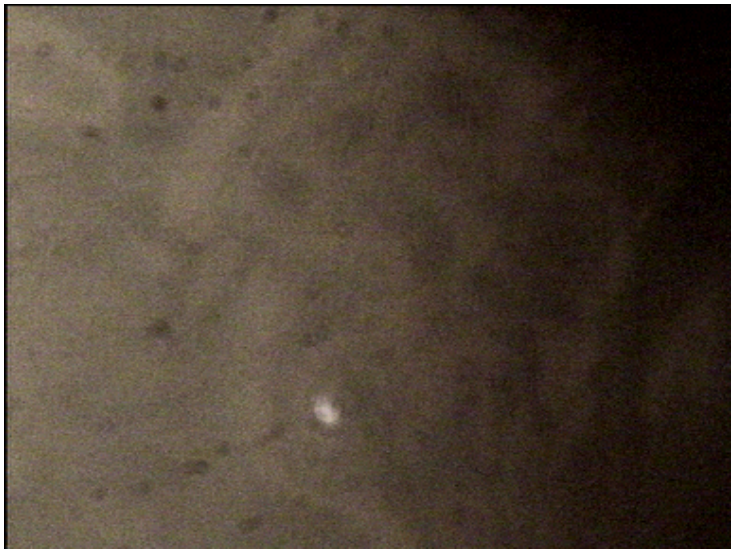

Figure 39: Sample MH2-Q3-210 B2 Line mapping start position. Picture is from the camera inserted into the detection path by use of a flip mirror, and sample illuminated by white light. The bright spot is reflections from the pumping laser.

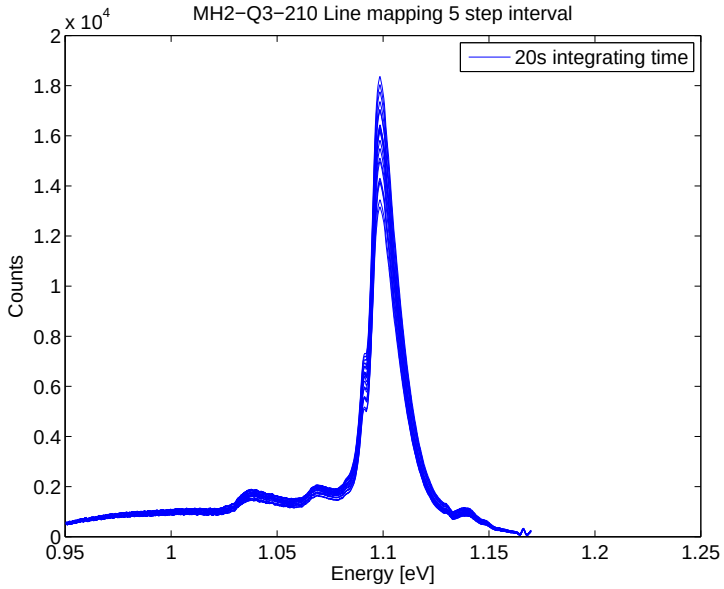

Figure 40: Sample MH2-Q3-210 B2 pumped with 170mW at 14K line map using 20 steps exactly 5 times larger than in figure 36.

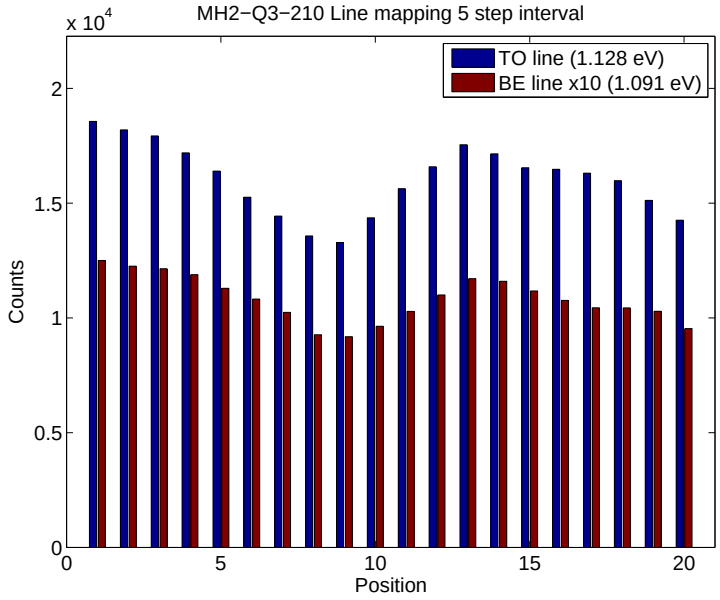

Figure 41: Sample MH2-Q3-210 B2 pumped with 170mW at 14K line map using 20 small steps exactly 5 times larger than in figure 36, looking at TO and BE line only from results in figure 40.

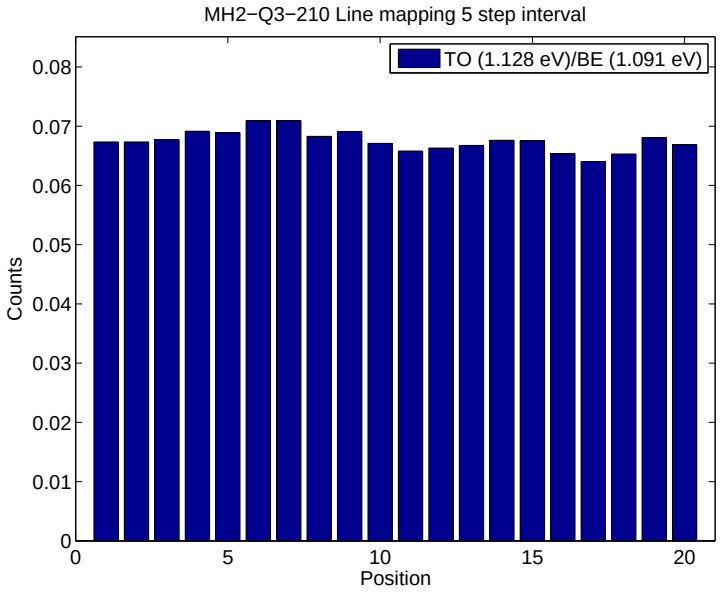

Figure 42: Sample MH2-Q3-210 B2 comparing relative intensity between TO and BE line from results in 41.

References

[1] B. G. Streetman and S. K. Banerjee, *Solid state electronic devices*. Prentice Hall, 2006.

[2] B. Jalali, "Physics and technology forefronts - silicon lasers," *American Physical Society*, 2006.

[3] B. Sopori, P. Rupnowski, V. Mehta, V. Budhraja, S. Johnston, N. Call, H. Moutinho, M. Al-Jassim, A. Shaikh, M. Seacrist, and D. Carlson, "Performance limitations of mc-si solar cells caused by defect clusters," *Conference Paper NREL/CP-520-45012*, 2009.

[4] N. A. Drozdov, A. Patrin, and V. Tkachev, "Recombination radiation on dislocations in silicon," *Pis'ma Xh. Eksp. Teor. Fiz.*, 1976.

[5] W. Lee, J. Chen, B. Chen, J. Chang, and T. Sekiguchi, "Cathodoluminescence study of dislocation-related luminescence from small-angle grain boundaries in multicrystalline silicon," *Applied Physics Letters*, 2009.

[6] R. Sauer, J. Weber, and J. Stolz, "Dislocation-related photoluminescence in silicon," *Appl. Phys.*, 1985.

[7] H. Sugimoto, M. Inoue, M. Tajima, A. Ogura, and Y. Ohsita, "Analysis of intra-grain defects in multicrystalline silicon wafers by photoluminescence mapping and spectroscopy," *Japanese Journal of Applied Physics*, 2006.

[8] M. Suezawa, Y. Sasaki, and K. Sumino, "Dependence of photoluminescence on temperature in dislocated silicon crystals," *Physica Status Solidi*, 1983.

[9] V. Higgs, P. Kightley, P. Goodhew, and P. Augustus, "Metal-induced dislocation nucleation for metastable sige/si," *Appl. Phys. Lett.*, 1991.

[10] T. Sekiguchi and K. Sumino, "Cathodoluminescence study on dislocations in silicon," *J. Appl. Phys.*, 1995.

[11] V. Kveder, E. Steinman, S. Shevchenko, and H. Grimmeiss, "Dislocation-related electroluminescence at room temperature in plastically deformed silicon," *Phys. Rev. B*, 1995.

[12] K. Weronek, J. Weber, and R. Buchner, "Origin of d-band photoluminescence in silicon," *Springer Proceedings in Physics*, 1991.

[13] I. Tarasov, S. Ostapenko, C.Haessler, and E.-U. Reisner, "Spatially resolved defect diagnostics in multicrystalline silicon for solar cells," *Elsevier Science S.A*, 2000.

[14] W. Staiger, G. Pfeiffer, K. Weronek, A. Höpner, and J. Weber, "Dislocation-induced defect levels in silicon," *Materials Science Forum*, 1994.

[15] P. J. Dean, J. Haynes, and W. Flood, "New radiative recombination processes involving neutral donors and acceptors in silicon and germanium," *Physical Review Volume 161 Number 3*, 1967.

[16] I. Tarasov, S. Ostapenko, W. Seifert, M. Kittler, and J. Kaleis, "Defect diagnostics in multicrystalline silicon using scanning techniques," *Elsevier Science B.V.*, 2001.

[17] H. Sugimoto, K. Araki, M. Tajima, T. Eguchi, I. Yamaga, M. Dhamrin, K. Kamisako, and T. Saitoh, "Photoluminescence analysis of intragrain defects in multicrystalline silicon wafers for solar cells," *Journal of Applied Physics*, 2007.

[18] T. V. Arguirov, "Electro-optical properties of dislocations in silicon and their possible application for light emmiters," ., 2007.

[19] G. Davies, "The optical properties of luminescence centres in silicon," *Physics Report*, 1988.

[20] H. Conzelmann, K. Graff, and E. Weber, "Chromium and chromium-boron pairs in silicon," *Appl. Phys. A*, 1982.

[21] H. Conzelmann and J. Weber, "Photoluminescence from chromium-boron pairs in silicon," *Physica*, 1983.

[22] L. Patrick and W. Choyke, "Photoluminescence of ti in four sic polytypes," *Physical Review B*, 1974.

[23] A. van Kemenade and S. Hagen, "Proof of the involvement of ti in the low-temperature abc luminescence spectrum of 6h sic," *Solid State Communications*, 1974.

[24] J. Weber, H. Bauch, and R. Sauer, "Optical properties of copper in silicon: Excitons bound to isoelectronic copper pairs," *Physical Review B*, 1982.

[25] M. Càlão and M. do Carmo, "Luminescence from an iron related deep center in silicon," *Physica Scripta*, 1988.

[26] H. Mohring, J. Weber, and R. Sauer, "Photoluminescence of excitons bound to an isoelectronic trap in silicon associated with boron and iron," *Physical Review B*, 1983.

[27] G. Zoth and W. Bergholz, "A fast preparation-free method to detect iron in silicon," *J. Appl. Phys*, 1990.

[28] P. Gundel, M. C. Schubert, W. Kwapil, J. Schön, M. Reiche, H. Savin, M. Yli-Koski, J. A. S. ans Gema Martinez-Criado, W. Seifert, W. Warta, and E. R. Weber, "Micro-photoluminescence spectroscopy on metal precipitates in silicon," *Phys. Status Solidi RRL*, 2009.

[29] D. Macdonald, J. Tan, and T. Trupke, "Imaging interstitial iron concentrations in boron-doped crystalline silicon," *Journal of applied physics*, 2008.

[30] V. Higgs, M. Goulding, and P. Kightley, "Characterization of epitaxial and oxidation-induced stacking faults in silicon: The influence of transition-metal contamination," *Appl. Phys. Lett.*, 1992.

[31] J. Bailey and E. R. Weber, "Precipitation of iron in polycrystalline silicon," *Physica Status Solidi (a)*, 1993.

[32] E. C. Lightowlers and V. Higgs, "Luminescence associated with the presence of dislocations in silicon," *Physica Status Solidi (a)*, 1993.

[33] N. Drozdov and A. Fedotov, "Electron-hole drops in dislocational silicon," *Microelectronic Engineering 66*, 2002.

[34] S. Nihonyanagi and Y. Kanemitsu, "Enhanced luminescence from electron-hole droplets in silicon nanolayers," *Applied physics letters*, 2004.

[35] N. A. Drozdov, A. A. Patrin, and V. T. Tkachev, "Modification of the dislocation luminescence spectrum by oxygen atmospheres in silicon," *physica status solidi (a)*, 1981.

[36] M. Tajima, M. Tokita, and M. Warashina, "Photoluminescence due to oxygen precipitates distinguished from the d-lines in annealed si," *Materials Science Forum*, 1995.

[37] M. Inoue, H. Sugimoto, M. Tajima, Y. Ohshita, and A. Ogura, "Microscopic and spectroscopic mapping of dislocation-related photoluminescence in multicrystalline silicon wafers," *J. Mater Sci*, 2007.

[38] P. Gundel, M. C. Shubert, and W. Warta, "Origin of trapping in multicrystalline silicon," *Journal of applied physics*, 2008.

[39] M. Hystad, "The distribution and impact of chromium impurities in compensated sog-silicon," Master's thesis, The Norwegian University of Science and Technology, 2009.

[40] B. Sopori, "A new defect etch for polycrystalline silicon," *J. Electrochem. Soc.*, 1984.

[41] E. Palik., *Handbook of optical constants of solids*. 2001.

[42] R. Hammond, T. McGill, and J. Mayer, "Temperature dependence of the electron-hole-liquid luminescence in si," *Physical Review B*, 1975.

[43] A. Hare, G.Davies, and A.T.Collins, "The temperature dependence of vibronic spectra in irradiated silicon," *J. Phys. C: Solid State Phys.*, 1972.

[44] T. Arguirov, W. Seifert, and M. K. J. Reif, "Temperature behaviour of photoluminescence and electron-beam-induced current recombination behaviour of extended defects in solar grade silicon," *J. Phys: Condens*, 2002.

[45] R. Sauer, J. Weber, , and J. Stolz, "Dislocation-related photoluminescence in silicon," *Applied Physics*, 1985.

[46] V. V. Kveder, E. A. Steinman, S. A. Shevchenko, and H. G. Grimmeiss, "Dislocation-related electroluminescence at room temperature in plastically deformed silicon," *Phys. Rev. B*, 1995.

[47] K. Leosson, J. Jensen, J. Hvam, and W. Langbein, "Linewidth statistics of single ingaas quantum dot photoluminescence lines," 2000.

[48] T. Arguirov, W.Seifer, G. Jia, and M. Kittler, "Photoluminiscence study on defects multicrystalline silicon," *Semiconductors*, 2006.

[49] A. J. Kenyon, C. E. Chryssoua, C. W. Pitta, T. Shimizu-Iwayamab, D. E. Holec, N. Sharmad, and C. J. Humphreysd, "Broad-band and flash-lamp pumping of 1.53 μm emission from erbium-doped silicon nanocrystals," 2001.

[50] M. Inoue, H. Sugimoto, M. Tajima, Y. Ohshita, and A. Ogura, "Microscopic and spectroscopic mapping of dislocation-related photoluminescence in multicrystalline silicon wafers," *Mater Electron*, 2008.

[51] E. Katz, M. Koltun, and L. Polyak, "Polycrystalline silicon solar cells: Improvements in efficiency through hydrogen passivation," *Diffusion and Defect Data Pt.B: Solid State Phenomena*, 1996.

[52] T. Arguirov, W. Seifert, M. Kittler, and J. Reif, "Temperature behaviour of extended defects in solar grade silicon investigated by photoluminescence and ebic," *Elsevier B.V.*, 2003.

[53] S. Binetti, J. Libal, M. Acciarri, M. D. Sabatino, H. Nordmark, E. Øverlid, J. Walmsley, and R. Holmestad, "Study of defects and impurities in multicrystalline silicon grown from metallurgical silicon feedstock," *Materials Science and Egnineering B*, 2008.

[54] L. Patrick and W. Choyke, "Photoluminescence of ti in four sic polytypes," *Physical Review B*, 1974.

[55] M. Wagner, I. Ivanov, L. Storasta, J. Bergman, B. Magnusson, W. Chen, and E. Janzén, "Photoluminescence upconversion in 4h-sic," *Applied Physics Letters*, 2002.

[56] J. Dean, "Photoluminescence as a diagnostic of semiconductors," *Prog. Crystal growth charact.*, 1982.

[57] H. Conzelmann, "Photoluminescence of transition metal complexes in silicon," *Appl. Phys. A*, 1987.

[58] M. Kittler, W. Seifert, T. Arguirov, I. Tarasov, and S. Ostapenko, "Room-temperature luminescence andelectronbeam-induced current (ebic) recombination behaviour of crystal defects in multicrystalline silicon," *Solar Energy Materials and Solar Cells*, 2002.

[59] S. A. Shevchenko and A. N. Izotov, "Dislocation-induced photoluminescence in silicon crystals of various impurity composition," *Physics of the Solid State*, 2003.

[60] T. Trupke, R. A. Bardos, M. C. Schubert, and W. Warta, "Photoluminescence imaging of silicon wafers," *Applied Physics Letters*, 2006.

[61] J. Bauer, O. Breitenstein, and J.-P. Rakotoniaina, "Electronic activity of sic precipitates in multicrystalline solar silicon," *phys. stat. sol. (a)*, 2007.

[62] V. Karasuyk, A. Steele, A. Mainwood, E. Lightowlers, and G. Davies, "Ultrahigh-resolution photoluminescence studies of excitons bound to boron in silicon under uniaxial stress," *Physical Review B*, 1992.

[63] M. Kasemann, D. Grote, B. Walter, W. Kwapil, T. Trupke, Y. Augarten, R. Bardos, E. Pink, M. Abbott, and W. Warta, "Luminescence imaging for the detection of shunts on silicon solar cells," *Prog. Photovolt: Res. Appl.*, 2008.

[64] M. Kasemann, W. Kwapil, B. Walter, J. Giesecke, B. Michl, M. The, J. Wagner, J. Bauer, A. Schütt, J. Carstensen, S. Kluska, F. Granek, H. Kampwerth, P. Gundel, M. Schubert, R. Bardos, H. Föll, H. Nagel, P. Würfel, T. Trupke, O. Breitenstein, M. Hermle, W. Warta, and S. Glunz, "Progress in silicon solar cell characterization with infrared imaging methods," *23rd European Photovoltaic Solar Energy Conference*, 2008.

[65] S. McHugo, H. Hieslmair, and E. Weber, "Gettering of metallic impurities in photovoltaic silicon," *Appl. Phys. A*, 1996.

[66] S. Ostapenko, I. Tarasov, J. Kalejs, C. Haessler, and E. Reisner, "Defect monitoring using scanning photoluminescence spectroscopy in multicrystalline silicon wafers," *Semicond. Sci. Technol.*, 2000.

[67] S. Pizzini, M. Acciarri, E. Leoni, and A. L. Donne, "About the d1 and d2 dislocation luminescence and its correlation with oxygen segregation," *phys. stat. sol. (b)*, 2000.

[68] E. Steinman, A. Kenyon, and A. Tereshchenko, "Time-resolved measurements of dislocation-related photoluminescence bands in silicon," *Semicond. Sci. Technol.*, 2008.

[69] H. Sugimoto, M. Tajima, T. Eguchi, I. Yamaga, and T. Saitoh, "Photoluminescence analysis of intra-grain defects in cast-grown polycrystalline silicon wafers," *Materials Science in Semiconductor Processing*, 2006.

[70] M. Tajima, "Characterization of semiconductors by photoluminescence mapping at room temperature," *Journal of Crystal Growth*, 1990.

[71] B. H. Liesert, T. Gregorkiewicz, and C. Ammerlaan, "Photoluminescence studies on therman donors in boron- and aluminum-doped silicon," *Physical Review B*, 1991.

[72] E. Irion, N. Biirger, W. Kiirner, K. Thonke, R. Sauer, W. Zulehner, and G. Pensl, "Photoluminescence study of acceptor-carbon complexes in irradiated silicon - aluminum-related defects," *Appl. Phys. A*, 1988.

[73] I. G. G. N. Mishinova and Y. M. Suleimanov, "Low-temperature luminescence of silicon carbide crystals," *Zhurnal Prikladnoi Spektroskopii*, 1966.

[74] R. Sauer, "Evidence for bound multiple-exciton complexes in silicon," *Phys. Rev. Let.*, 1973.

[75] R. Sauer, "1974," *Solid State Communications*, Bound Multiple-Excition Complexes in Silicon at High Doping Levels.

A Silicon energy bands

Energy	Name	Temp.	Impurity / Defect	Observed in
0.735eV	ZPL	22K	Fe contamination	[25]
0.745eV	C-N		Carbon-Nitrogen complex	[19]
0.76-0.8eV	Defect	290K	Dislocation with low contamination	[13, 16, 48]
0.77-0.78eV	D_b	4.2-295K	Oxygen impurity band	[36, 37]
0.77eV	P line	12K	C-O complex related	[19, 53]
0.780eV	$CrB^{0\Gamma}$	4.2K	CrB^0 phonon replica	[21]
0.79eV	C-O	12K	Carbon-Oxygen complex	[19, 53, 43]
0.80eV	D1'	77K	Dislocations [1]	[13, 16]
0.812eV	D1	4.2K	Dislocation related line [1]	[4, 6, 52]
0.8160	CrB^2	4.2K	Cr-B excitation of local vibrations	[21]
0.8402	CrB^1	4.2K	Cr-B excitation of local vibrations	[21]
0.8432eV	CrB^0	4.2K	Cr-B pair no-phonon	[20, 21]
0.875eV	C-Ga		Carbon-Gallium complex	[19]
0.875eV	D2	4.2K	Dislocation related line [1]	[4, 6, 52]
0.89eV	D2'	77K	Dislocations [1]	[13, 16]
0.8-0.9eV	D_{a1}	11K	Broad background emission under D1/D2	[36]
0.91eV	H-line	12K	C-O complex related	[19, 53]
0.93eV	H-line	12K	C-O complex related	[19, 53]
0.934eV	D3	4.2K	Dislocations [2]	[4, 6, 52]
0.95eV	D3'	77K	Dislocations [2]	[13, 16]
0.953eV	D5	4.2K	Straight dislocations	[6, 12]
0.9537eV	Defect	300K	Iron precipitate	[28]
0.968eV	I^{TO+20^Γ}	26K	TO + 2 Zone center phonon	[15]
0.969eV	C-C		Carbon-Carbon complex	[19]
0.98eV	R2BB	80K	Two phonon replica of band edge emission	[52]
0.9-1.0eV	D_{a2}	11K	Broad background emission under D3/D4	[36]
1.000eV	D4	4.2K	Dislocations [2]	[4, 6, 52]
1.00eV	D4'	77K	Dislocations [2]	[13, 16]
1.0089eV	FeB^0(TO)	6K	Fe-B pair phonon replica	[26]
1.0126eV	D6	4.2K	Stacking faults	[6, 12]
1.013eV	$I^{TO+0^\Gamma+IV^a}$	26K	$TO + 0^\Gamma + IV^a$ phonon	[15]
1.014eV	Cu_0	4.2K	Copper doping	[24, 12]
1.018eV	W/I1		Radiation damage	[19]
1.0315eV	I^{TO+0^Γ}	26K	TO + Zone center phonon	[15]
1.04eV	R1BB	80K	One phonon replica of band edge emission	[52]
1.045eV	Q		4-Li atom complex	[19]
1.0504eV	FeB^2	6K	Fe-B pair contamination	[26]

Continued on next page

Table 5 – continued from previous page

Energy	Name	Temp.	Impurity / Defect	Observed in
1.051eV	I^{TO+IV^b}	26K	Inter valley phonon replica	[15]
1.0595eV	FeB^1	6K	Fe-B pair contamination	[26]
1.0692eV	FeB^0	6K	Fe-B pair no phonon	[26]
1.074eV	I^{TO+IV^a}	26K	Inter valley phonon replica	[15]
1.078	EHD	4.2K	Electron Hole Droplet dislocation-area	[33]
1.082eV	EHD_{TO}	4.2K	Electron Hole Droplet dislocation-free	[42, 33, 34]
1.0835eV	In^{TO}	30K	Indium doping TO	[15]
1.0888eV	Bi^{TO}	15K	Bismuth doping TO	[15]
1.0902eV	Al^{TO}	30K	Aluminum doping TO	[15]
1.0907eV	As^{TO}	15K	Arsenic doping TO	[15]
1.0907eV	Ga^{TO}	15K	Gallium doping TO	[15]
1.0916eV	P^{TO}	15K	Phosphorus doping TO	[15]
1.092eV	BE1	4.2K	Boron bound exciton	[4, 74, 75]
1.0921eV	Sb^{TO}	15K	Antimony doping TO	[15]
1.0970eV	I^{TO}/FE	26K	Transversal Optical/Free exciton	[15, 42, 33]
1.0924eV	B^{TO}	15K	Boron doping TO	[15]
1.093eV	B_{TO}	4.2K	TO phonon replica of Boron bound exciton	[17, 37]
1.1365eV	I^{TA}/LO/FE	26K	Transversal Acoustic/Longitudinal/FE	[42, 15]
1.147eV	BE2	2K	Phosphorous bound exciton	[74, 75]
1.1545eV	I^0	26K	No phonon	[15]
2.786eV	$^4 8_C$Ti	4.2K	C line Ti isotope 48 impurity in 6H SiC	[23]
2.820eV	$^4 8_B$Ti	4.2K	B^0 line Ti isotope 48 impurity in 6H SiC	[23, 55]
2.85eV	^{4}8Ti	4.2K	Ti isotope 48 impurity in 4H SiC	[22]
2.861eV	$^4 8_A$Ti	4.2K	A^0 line Ti isotope 48 impurity in 6H SiC	[23, 55]

Table 5: Silicon energy bands

[1] D1 and D2: It has been argued that they originate in electronic transition at the geometrical kinks on dislocations [8], point defects [6] and impurities [9] and/or from the reaction products of dislocations [10].

[2] D3 and D4 lines is generally thought to be related to electronic transition within dislocation cores [11]. In addition, it has been suggested that the D3 line most likely is a phonon-assisted replica of D4 [11].

B Sample types and procedures

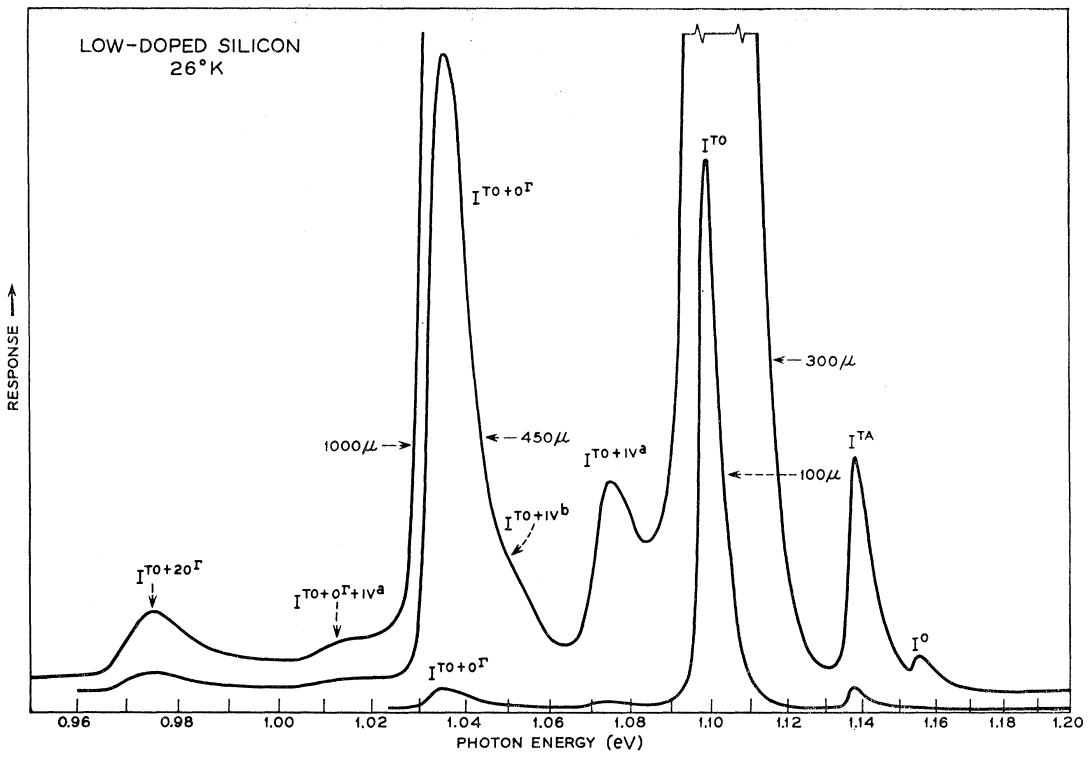

Figure 43: Intrinsic/low doped ($2 \cdot 10^{14} cm^{-3}$ P atoms) Si PL specter from [15]

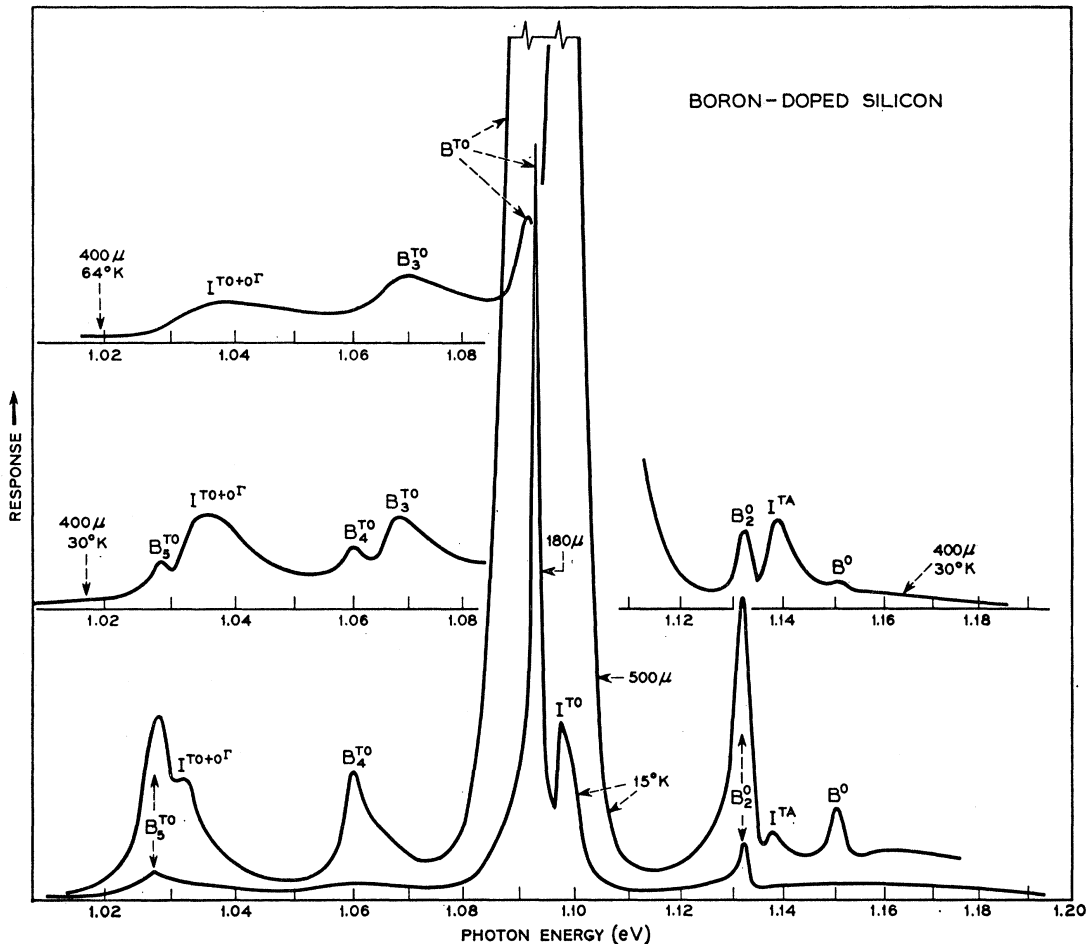

Figure 44: Boron doped ($6 \cdot 10^{16} cm^{-3}$) Si PL specter from [15]

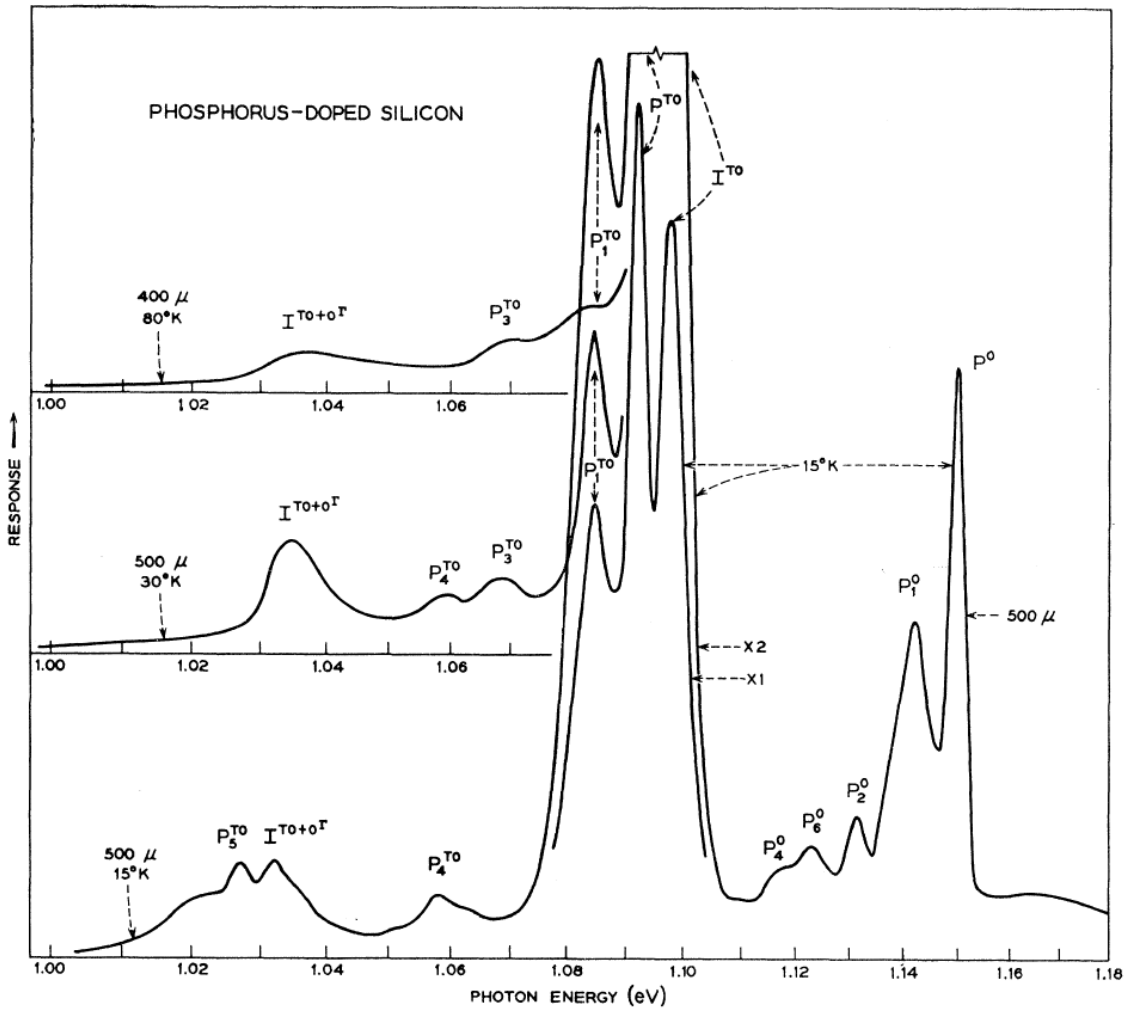

Figure 45: Phosphorus doped ($8 \cdot 10^{16} cm^{-3}$) Si PL specter from [15]

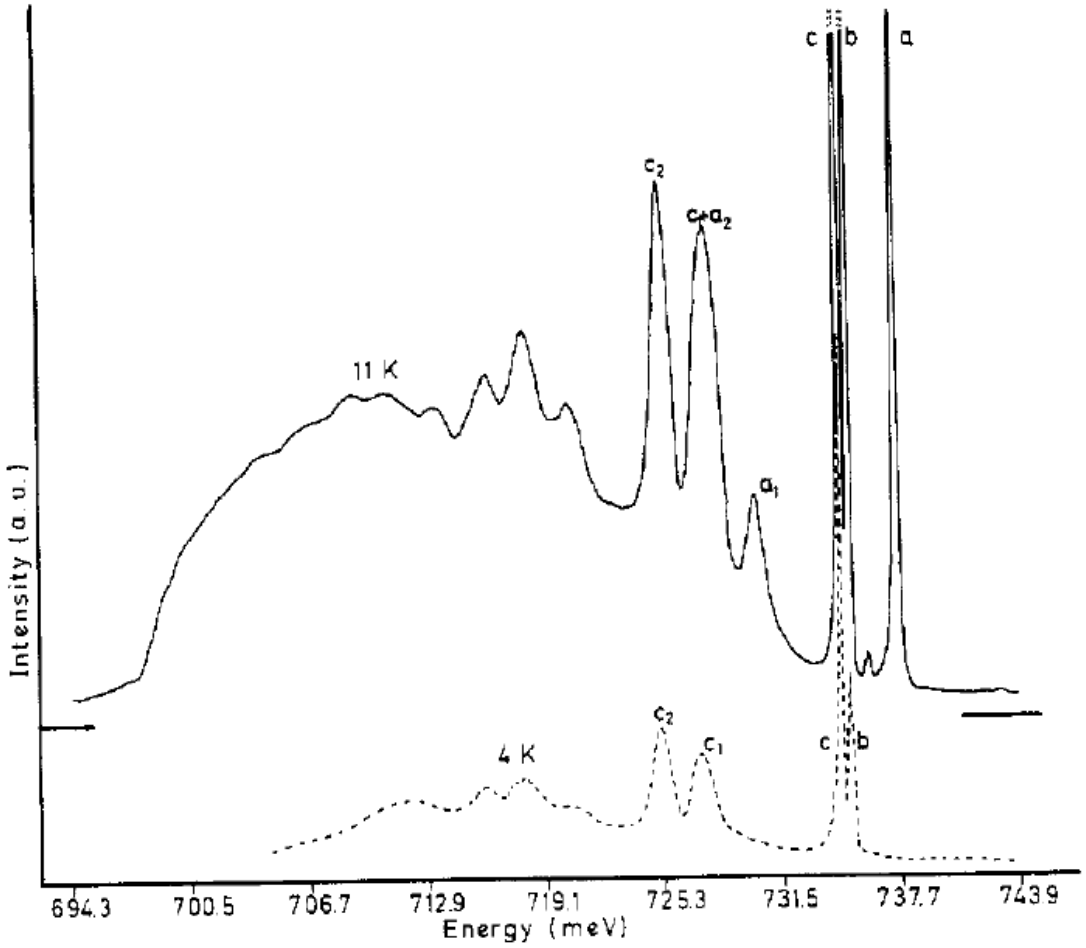

Figure 46: Iron diffused Si sample at two different temperatures from [25]

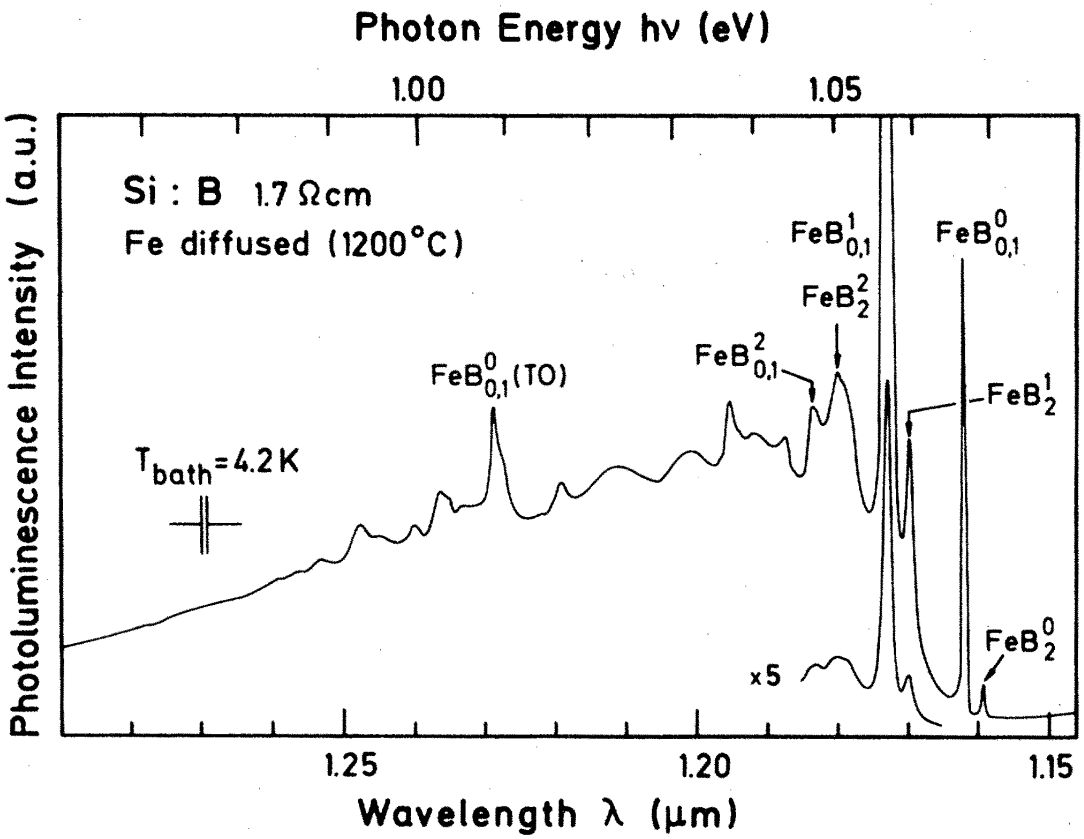

Figure 47: Iron diffused boron doped Si sample from [26]

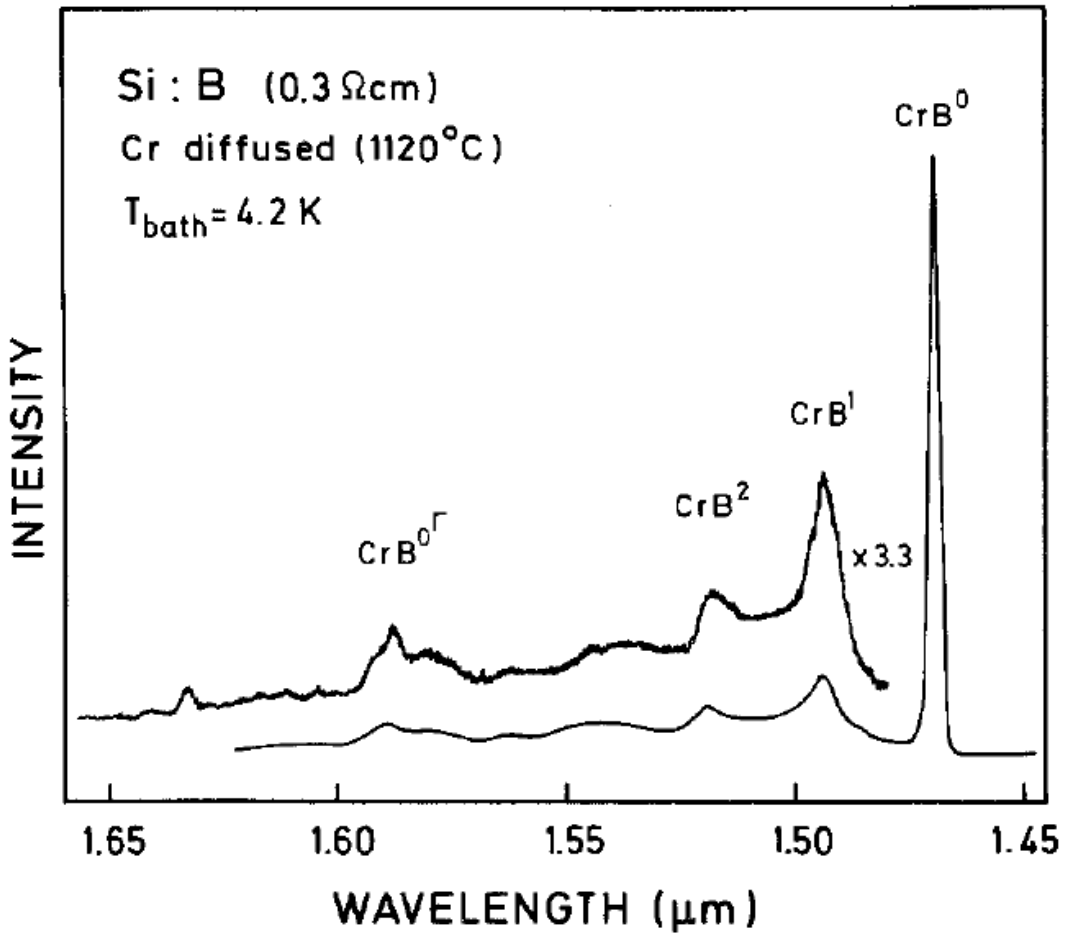

Figure 48: Chromium diffused Boron doped Si sample from [21]

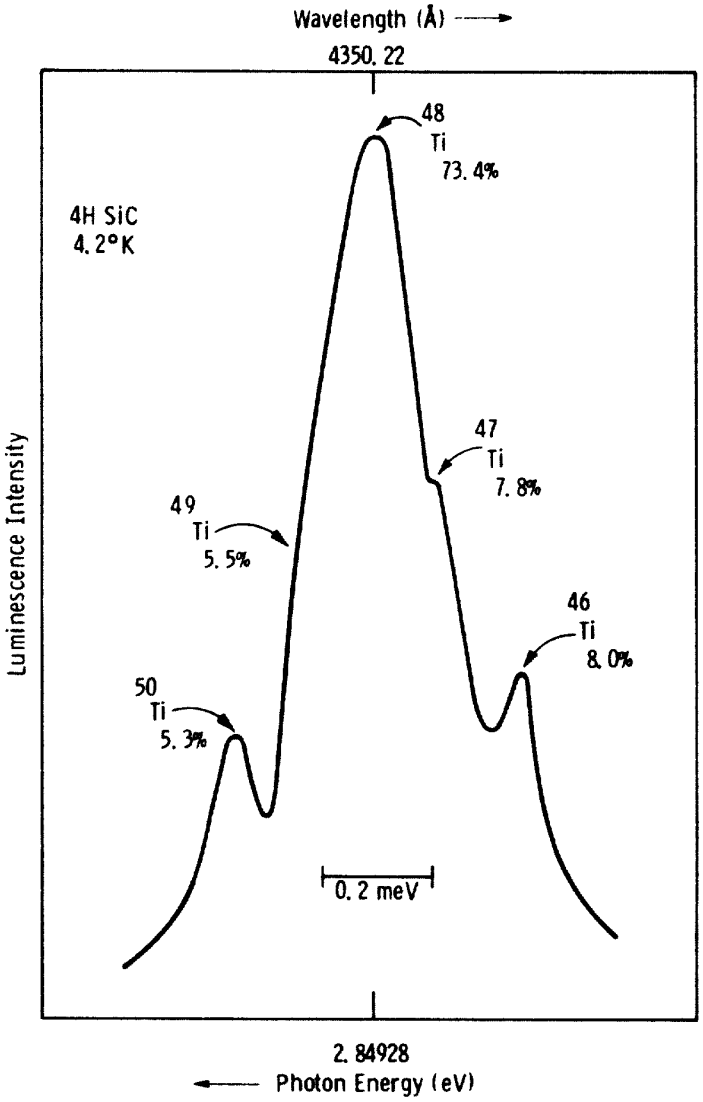

Figure 49: Titanium PL from Ti contaminated 4H SiC

Ref.	Sample type	Excitation process	Area	Processing	Doping
[17]	mc-Si	532nm Nd:YVO_4	$0.1mW/10\ \mu$m diameter	Sawing damage etched by HNO_3/HF	B-doped
[36]	Cz-Si	Kr ion laser 647nm	10 μm		Undoped
[4]	Cz-Si	Xenon lamp	50mW on 3mm modulated at 9Hz	deformed by bending at 850° C	undoped, weak n and p
[13]	mc-Si	800nm AlGaAs laser	Pulsed 300mW / 3mm		Block-casting technique for Baysix
[16]	mc-Si	800nm AlGaAs at 140mW		Produced by EFG	
[52]	mc-Si and FZ-Si	Ar ion 514nm at 300mW	100μm	Produced by EFG	boron doped $10^15cm^{-}1$
[6]	FZ-Si	Kr-ion 647nm, Ar-ion 415nm and Nd-YAG 1064nm		Deformed a 650° C and 850° C	residual 10^{12}cm^{-3} boron
[37]	mc-Si	Nd:YVO 532nm	6mW, 10μm diameter	Slicing damage etched off by HNO_3/HF	boron doped
[21]	FZ-Si and CZ-Si		50mW laser	Etched with HNO_3/HF. Chromium diffused	boron doped
[26]	FZ-Si	Ar+ 514nm	500mW	Fe diffused	boron doped
[25]	FZ-Si	Argon laser		Fe diffusion	undoped
[24]		Ar^+ 514nm at 1.5W			Cu doped
[12]	FZ-Si	Ar^+ 514nm		Heated above a Bunsen burner	Doped with Cu and/or Fe
[53]	mc-Si		6W/cm^2	Polished by HNO_3/HF	Undoped
[15]	CZ-Si	200W mercury arc 2.5eV			Undoped and doped
[33]		Ar^+ or Kr^+ laser 0.6W	0.8mm diameter	Dislocations by bending at 700°C	phosphorus doped

Table 6: Sample types and procedures

C Abbrevations

Abbrevation	Description
B_{TO}	TO phonon replica of the Boron bound exiton
BE	Bound exciton
D_a	Broad background emission
D_b	Oxygen impurity band
CZ-Si	Czochralski processed Silicon
D1	Dislocation related line 1
D1'	Dislocation related line 1 for mc-Si
D2	Dislocation related line 2
D2'	Dislocation related line 2 for mc-Si
D3	Dislocation related line 3
D3'	Dislocation related line 3 for mc-Si
D4	Dislocation related line 4
D4'	Dislocation related line 4 for mc-Si
EBIC	Electron beam induced current
EBSP	Electron Backscatter Diffraction Pattern
EHD	Electron Hole Droplet
FE	Free exciton
FZ-Si	Float-zone silicon
EFG	Edge-define Film-fed Growth
mc-Si	Multicrystalline silicon
R1BB	One phonon replica of band edge emission
R2BB	Two phonon replica of band edge emission
SA GB	Small Angle Grain Boundary
ZPL	Zero Phonon Line

Table 7: Abbreviations

D Matlab code

D.1 Dead pixel correction

```
function [C] = dead_pixel_correction(A)
% Copy neighbour value on defect pixels in InGaAs camera.
    C = A;
    C(401,2) = A(400,2); % Defective (slightly to low)
    C(723,2) = A(722,2); % Defective (slightly to high)
    C(933,2) = A(932,2); % This pixel is dead (too high values)
    C(873,2) = A(872,2); % This pixel is dead (too low values)
end
```

D.2 Dark current noise estimation removal

```
function[C] = dark_current_noise_removal(A,B)
% Smoothends noise, and find min value, and remove offset.
% Negative values from noise are truncated to 0.
% A and B MUST be of equal length!

    if (length(A) ~= length(B))
        X = 'Length different from B';
        B = [];
    end
    if (isempty(B))
        % No noise is measured, remove a static offset instead.
        C = A;
        Ay = A(:,2); % Amplitude values
        Ay = sgolayfilt(Ay,1,255); % 1st order filtering
        offset = min(Ay); % Minimum offset, from noise averaging

        for i=1:length(A),
            new_value = A(i,2)-offset;
            if (new_value < 0)
                new_value = 0;
            end
            C(i,2) = new_value;
        end
    else
        % B matrix is the noise measurement
        % - filter, and remove offset
        C = A;
        By = B(:,2); % Amplitude values
        OFFSET = sgolayfilt(By,1,25); % 1st order filtering
```

```
        for i=1:length(A),
            new_y_value = (C(i,2) - OFFSET(i));
            % white noise artifacts can result in < 0 values which are
            % clearly not possible in real life
            if (new_y_value < 0)
                new_y_value = 0;
            end
            C(i,2) = new_y_value;
        end
    end
end
```

D.3 Read result files from directory

```
function [C] = get_result_from_dir(dname,delimiter,drop_rightside)
% Reads all files in a directory, and return matrix elements
% separated by delimiter from file contents

    C = 0;

    % Read directory
    files = dir(dname);

    % Sort filenames in dir
    filenames = {files.name};

    % Sort numbers in string logically
    [dummy, index] = sort_nat(filenames);

    % re-index the files array:
    files = files(index);

    % Combine files to one large array
    for i=1:length(files),
       if (files(i).name == '.') % Do nothing
       elseif (strcmp(files(i).name,'..')) % Do nothing
           elseif (strcmp(files(i).name,'.svn')) % Do nothing
       else
           % Read file contents into memory
           A = dlmread([dname,files(i).name],delimiter);

           % Filter out dead pixels in the InGaAs camera
           A = dead_pixel_correction(A);
           if (0 == C)
               C=A;
```

```
            else
                if (drop_rightside == 0)
                    C = matrix_align_and_glue(C,A);
                else
                    C = matrix_align_and_glue_reverse(C,A);
                end
            end
        end
    end
end
```

D.4 Remove overlap and glue intervals

```
function[C]  = matrix_align_and_glue_reverse(A,B)

overlapIndex = 0;

% Drop the left side in the interval
    for i=1:length(B),
        if (A(length(A),1) < B(i,1))
           overlapIndex = i;
           break;
        end
    end

    % Define new array length
    sizeA = length(A);
    sizeB = length(B);
    new_array_size = (sizeA+sizeB-overlapIndex);

    % Define right length of array
    temp_C = zeros([new_array_size 2]);

    % Add existing elements
    for j = 1:length(A),
        temp_C(j,1) = A(j,1);
        temp_C(j,2) = A(j,2);
    end

    % Add new elements
    for k = 1:(length(B)-overlapIndex),
       temp_C((length(A)+k),1) = B(overlapIndex+k,1);
       temp_C((length(A)+k),2) = B(overlapIndex+k,2);
    end

    C = temp_C;
```

```
end
```

D.5 Filter and plot results

```
function plot_result(Result,fig_number,type,legend1,title1,fontsize,plot_type,sgofi

    % Define X and Y values
    Ax = Result(:,1);
    Ay = Result(:,2);

    % Filter
    if (sgofilter_strength > 0)
        % 1st order filtering
        Ay = sgolayfilt(Ay,1,sgofilter_strength);
    end

    % Calculate eV values if needed
    if (strcmp(type,'ev'))
        Ax = nm_to_ev(Ax);
        xlabel1 = 'Energy [eV]';
    else
       xlabel1 = 'Wavelength [nm]';
    end

    % Detect same figure plot
    cf = get(0,'CurrentFigure');
    fill_info = 0;
    if (isempty(cf))
        fill_info = 1;
    end
    if (cf ≠ fig_number)
       fill_info = 1;
    end

    % Plot
    fig = figure(fig_number);

    if (fill_info)
        axes1 = axes('Parent',fig,'FontSize',fontsize);
        box(axes1,'on');

        hold(axes1,'all');
        hold on;
    end

    plot(Ax,Ay,plot_type);
```

```
    % If no figure exists, input info
    if (fill_info) % Don't add info twice
        legend(legend1);
        title(title1);
        ylabel('Counts');
        xlabel(xlabel1);
    end
end
```